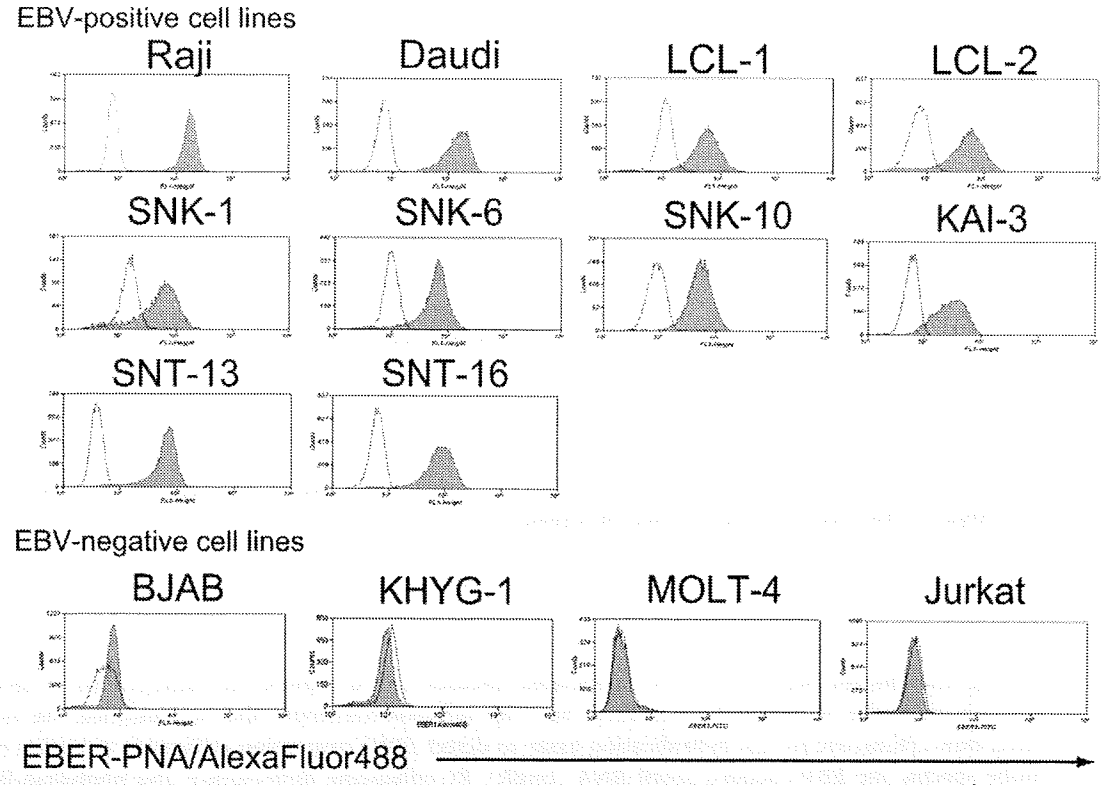

Figure 1. Detection of Epstein-Barr virus (EBV)–encoded small RNA (EBER) by flow cytometric in situ hybridization assay. EBV^+ or EBV^- cells were fixed, permeabilized, and hybridized with either the EBER peptide nucleic acid (PNA) probe *(shaded histograms)* or the negative control PNA probe *(open histograms)*. After enhancement of fluorescent signals with Alexa Fluor 488–labeled antibodies, cells were analyzed by flow cytometry. Cell lines included the EBV^+ B cell lines, Raji, Daudi, lymphoblastoid cell line (LCL) 1, and LCL-2; EBV^+ natural killer (NK) cell lines, SNK-1, SNK-6, SNK-10, and KAI3; EBV^+ T cell lines, SNT-13 and SNT-16; EBV^- B cell line, BJAB; EBV^- NK cell line, KHYG-1; EBV^- T cell lines, MOLT-4 and Jurkat. FITC, fluorescein isothiocyanate.

ever, biopsies are invasive and cannot always be performed, owing to the lack of nodal sites or difficulty of access. Because EBV-infected lymphocytes migrate in the peripheral blood in most EBV-associated lymphomas or lymphoproliferative diseases, peripheral blood lymphocytes can be examined instead of tissue specimens [7]. For this reason, applying EBER ISH to peripheral blood would allow EBV-infected cells to be identified and quantified using a more convenient and less invasive procedure.

Peptide nucleic acid (PNA) is a DNA/RNA analog capable of binding to DNA and RNA in a sequence-specific manner [10]. In PNA, nucleobases are attached to a backbone that consists of repetitive units of N-(2-aminoethyl)glycine, in contrast to the sugar-phosphate backbone of DNA/RNA. Because of the high binding affinity of PNA to DNA/RNA and its stability [11, 12], PNA probes have been used for fluorescent ISH to determine telomere lengths at chromosome ends [13–15].

In this study, we established a novel ISH method to detect $EBER^+$ suspension cells with flow cytometry using a commercially available EBER PNA probe [16]. By enhancing fluorescence and photostability and modifying the fixation and hybridization steps, we successfully stained both EBER and surface antigens. With this novel flow cytometric ISH (FISH) method, we showed that EBV^+ $\gamma\delta$ T cells were present in the peripheral blood of patients with hydroa vacciniforme–like lymphoproliferative disease [17], which was defined as an EBV^+ cutaneous T cell lymphoproliferative disease that occurs in children [6, 18].

METHODS

Cell lines. The EBV^+ B cell lines included Raji and Daudi, both of which were derived from Burkitt's lymphoma tissue, and 2 lymphoblastoid cell lines transformed with B95–8 EBV. BJAB, an EBV^- B cell line, was used as a negative control. The EBV^+ T cell lines included SNT-13 and SNT-16 [19], and the EBV^+ NK cell lines included SNK-1, -6, and -10 [19], and KAI3 [20]. These T and NK cell lines were derived either from patients with chronic active EBV infection or from T or NK cell lymphomas. MOLT-4 and Jurkat were used as EBV^- T cell lines [21], and KHYG-1 was used as an EBV^- NK cell line [22].

Patients and samples. Three patients with hydroa vaccini-

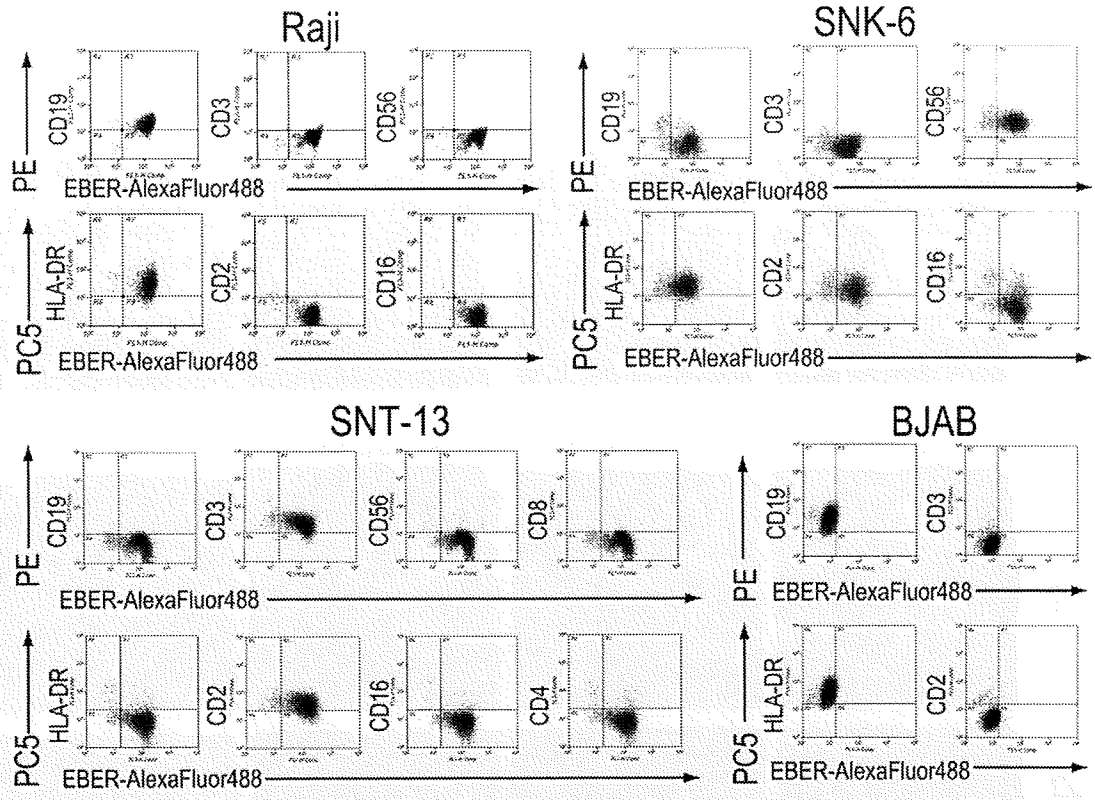

Figure 2. Dual staining for surface antigens and Epstein-Barr virus (EBV)–encoded small RNA (EBER) by flow cytometric in situ hybridization assay. Cells were stained for surface antigens with phycoerythrin (PE)– or PE–cyanin 5 (PC5)–labeled monoclonal antibodies and then fixed, permeabilized, and hybridized with the EBER peptide nucleic acid probe. After enhancement of fluorescent signals, cells were analyzed by flow cytometry. The EBV$^+$ B cell line was Raji; the EBV$^+$ natural killer (NK) cell line, SNK-6; the EBV$^+$ T cell line, SNT-13; and the EBV$^-$ B cell line, BJAB.

forme–like lymphoproliferative disease and 1 patient with post-transplantation lymphoproliferative disease were enrolled in the study. As negative controls, 5 healthy volunteers who were seropositive for EBV were also enrolled. Heparinized blood samples were obtained, and peripheral blood mononuclear cells (PBMCs) were separated by density gradients. PBMCs were cryopreserved at −80°C until analysis.

Informed consent was obtained from all patients or guardians and healthy carrier donors. The institutional review board of Nagoya University Hospital approved the use of all specimens examined in this study.

Surface marker staining. Cells were stained with phycoerythrin (PE)–labeled anti-CD3 (clone UCHT1; eBioscience), anti-CD8 (clone B9.11; Immunotech), anti-CD19 (clone HD37; Dako, and anti-CD56 (clone N901; Immunotech) monoclonal antibodies and PE–cyanin 5 (PC5)–labeled anti-CD2 (clone 39C1.5; Immunotech), anti-CD4 (clone 13B8.2; Immunotech), anti-CD16 (clone 3G8; Immunotech), anti-CD56 (clone N901; Immunotech), anti–HLA-DR (clone IMMU357; Immunotech), anti-$\alpha\beta$ T cell receptor (TCR) (clone IP26; eBioscience), and anti-TCR$\gamma\delta$ (clone IMMU510; Immunotech) monoclonal antibodies for 1 h at 4°C. Isotype-matched monoclonal mouse immunoglobulin (Ig) G antibodies were used in each experiment as controls.

PNA probes. The EBER PNA probe, Y5200, was purchased from Dako. The Y5200 probe is a mixture of 4 different fluorescein-labeled PNA probes complementary to EBER [16]. The negative control PNA probe (Dako), which consists of fluorescein-conjugated random PNA probes, was used as a negative control. The positive control PNA probe (Dako) directed against glyceralaldehyde 3-phosphate dehydrogenase was used as a positive control. Each PNA probe was labeled with fluorescein isothiocyanate (FITC).

FISH technique. The following experiments were performed in 1.5-mL microcentrifuge tubes (Corning). For surface marker staining, cells were stained with the appropriate antibodies before fixation and hybridization. Cultured cells (2×10^5) or PBMCs (5×10^5) were fixed with 1% (vol/vol) acetic acid in 4% paraformaldehyde/phosphate buffered saline (PBS) for 40 min at 4°C. After being washed once with PBS, cells were permeabilized in 50 μL of 0.5% Tween 20/PBS at room temperature. Formamide, buffer, and water were added to the cells in permeabilization buffer so that the final formamide and buffer concentrations were the same as the hy-

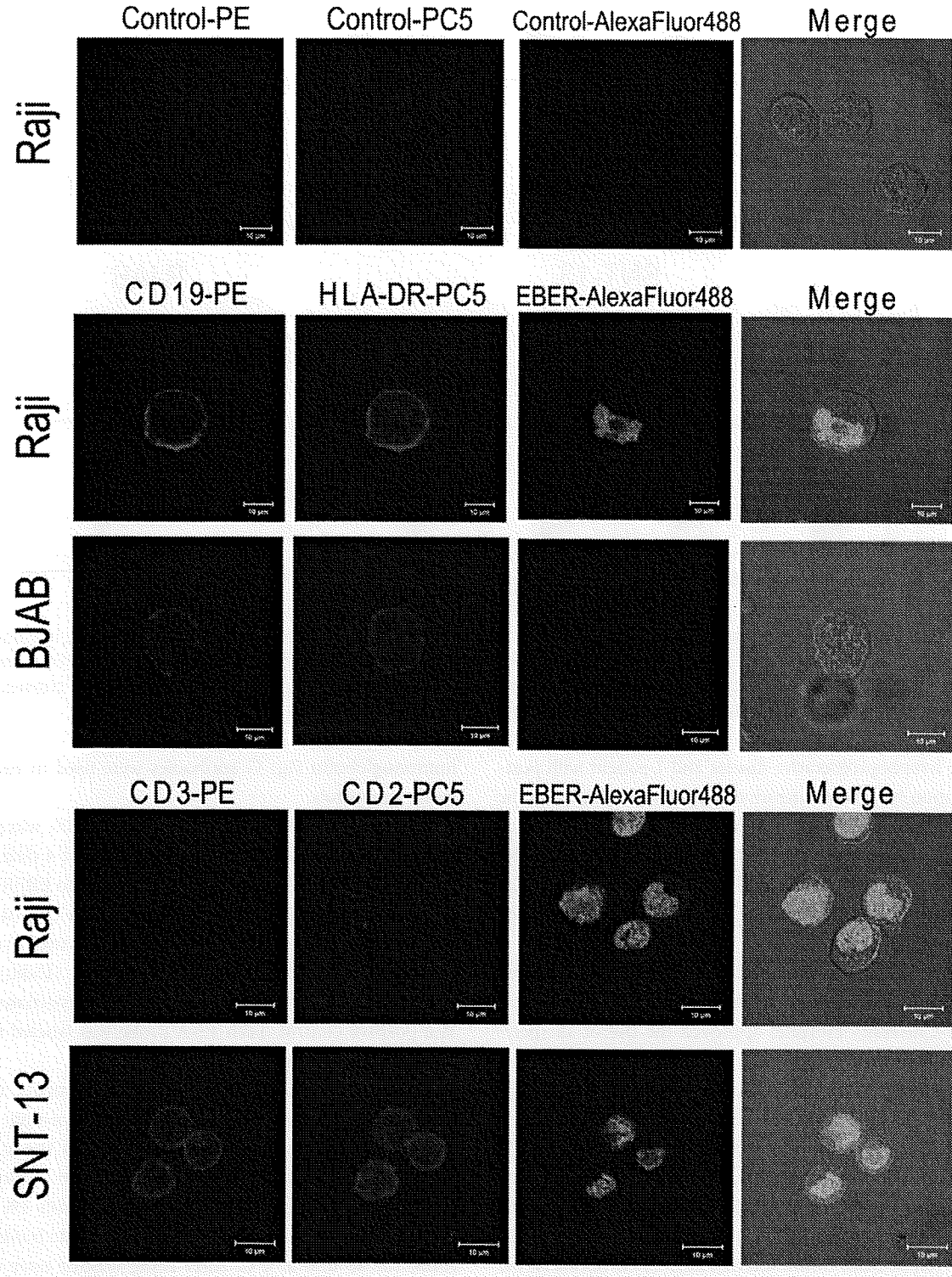

Figure 3. Detection of dual staining for surface antigens and Epstein-Barr virus (EBV)–encoded small RNA (EBER) by confocal microscopy. Cells were stained for surface antigens with phycoerythrin (PE)– or PE–cyanin 5 (PC5)–labeled monoclonal antibodies and then fixed, permeabilized, and hybridized with the EBER peptide nucleic acid probe. After enhancement of fluorescent signals, cells were mounted on glass slides and analyzed by confocal immunofluorescence microscopy. The EBV^+ B cell line was Raji; the EBV^- B cell line, BJAB; and the EBV^+ T cell line, SNT-13. Bars, 10 μm.

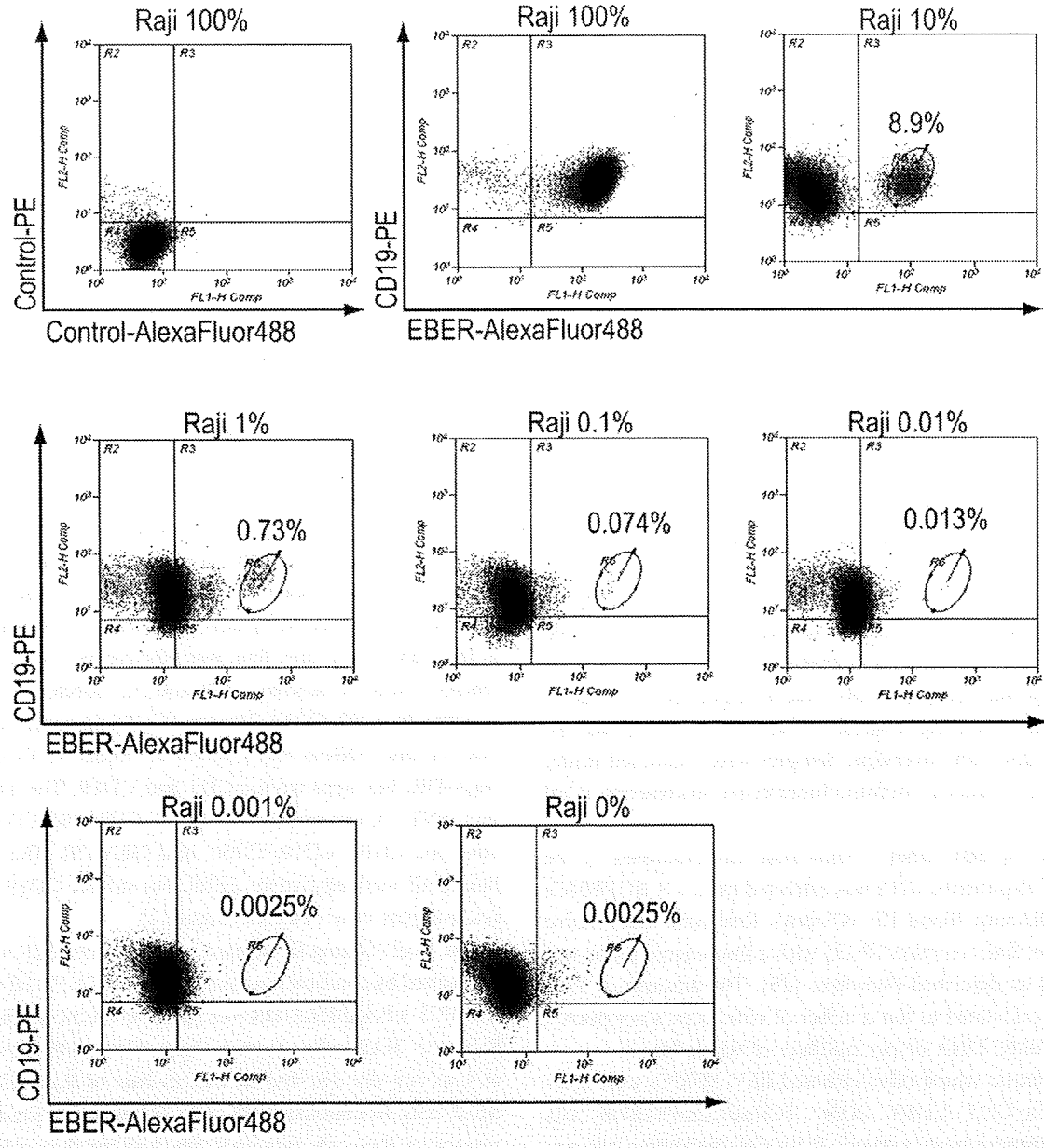

Figure 4. Minimum detection level of cells positive for Epstein-Barr virus (EBV) by flow cytometric in situ hybridization assay. EBV$^+$ Raji cells and EBV$^-$ BJAB cells were mixed at various ratios, stained with phycoerythrin (PE)–labeled anti-CD19 antibody, and then fixed, permeabilized, and hybridized with the EBV-encoded small RNA (EBER) peptide nucleic acid (PNA) probe. After enhancement of fluorescent signals, the cells were analyzed by flow cytometry. The ratio of Raji to BJAB cells is shown above each quadrant. Numbers in quadrants indicate percentages of CD19$^+$EBER$^+$ cells.

bridization solution (6% [wt/vol] dextran sulfate, 10 mmol/L sodium chloride, 17.5% [vol/vol] formamide, 0.061% [wt/vol] sodium pyrophosphate, 0.12% [wt/vol] polyvinylpyrrolidone, 0.12% [wt/vol] Ficoll, 5 mmol/L disodium ethylenediaminetetraacetic acid, 50 mmol/L tris(hydroxymethyl) aminomethane [pH 7.5]). The cells were resuspended in 45 μL of hybridization solution containing 12 nmol/L of the EBER PNA probe, negative control PNA probe, or positive control PNA probe, all FITC labeled. Hybridization was carried out for 1 h at 56°C. Then cells were washed twice (for 10 and 30 min) with 0.5% Tween 20/PBS at 56°C. To enhance fluorescence and photostability, the Alexa Fluor 488 Signal Amplification Kit (Molecular Probes) was used. The kit protocol had 2 steps, using Alexa Fluor 488 rabbit anti-FITC to bind FITC-labeled probes and Alexa Fluor 488 goat anti-rabbit IgG for further enhancement.

Stained cells were analyzed using a FACSCalibur flow cytometer and CellQuest software, version 5.2.1 (Becton Dickinson). For cell lines, live gating was determined by forward

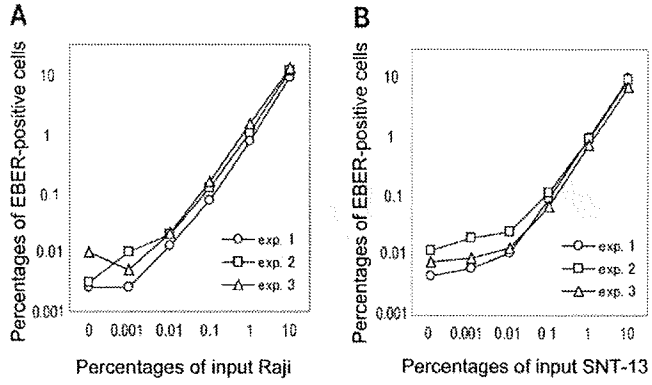

Figure 5. Correlation between the percentage of cells positive for Epstein-Barr virus (EBV)–encoded small RNA (EBER) and input EBV$^+$ cells. EBV$^+$ and EBV$^-$ cells were mixed at various ratios and analyzed by flow cytometric in situ hybridization assay. Each experiment (exp.) was done in triplicate. *A*, B cell lines included Raji (EBV$^+$) and BJAB (EBV$^-$). *B*, T cell lines included SNT13 (EBV$^+$) and Jurkat (EBV$^-$).

and side scatter profiles. For PBMCs, lymphocytes were gated by standard forward and side scatter profiles [23]. Up to 50,000 events were acquired for each analysis.

Confocal microscopy. Cells were resuspended in 20 μL of PermaFluor mounting medium (Thermo) and mounted onto glass slides with coverslips. Samples were examined under an LSM 510 confocal immunofluorescence microscope (Carl Zeiss) [24].

Analyses of EBV DNA. Viral load was examined in the PBMCs of all patients. DNA was extracted from 1×10^6 PBMCs using a QIAamp Blood Kit (Qiagen). Real-time quantitative polymerase chain reaction (PCR) with a fluorogenic probe was performed as described elsewhere [25]. The amount of EBV DNA was calculated as the number of virus copies per microgram of PBMC DNA or per milliliter of whole blood.

To determine which cells harbored EBV, PBMCs were fractionated into CD3$^+$, CD19$^+$, CD56$^+$, TCR$\alpha\beta^+$, and TCR$\gamma\delta^+$ cells using an immunobead method (IMag Cell Separation System; Becton Dickinson) with 97%–99% purity. The fractionated cells were analyzed by real-time quantitative PCR and compared with PBMCs [26]. The clonality of EBV was determined using Southern blotting with a terminal repeat probe, as described elsewhere [27].

Rearrangement of the TCR gene. TCR gene rearrangement was determined by multiplex PCR assays using the T Cell Gene Rearrangement/Clonality assay (InVivoScribe Technologies), which was developed and standardized in a European BIOMED-2 collaborative study [28, 29].

RESULTS

FISH assay to detect EBER. EBV$^+$ or EBV$^-$ cell lines were fixed, permeabilized, and hybridized with the EBER PNA probe or negative control PNA probe. After enhancement of fluorescent signals, cells were analyzed by flow cytometry. On the basis of flow cytometry, Raji cells had a significant increase in fluorescence intensity of the EBER PNA probe compared with the negative control PNA probe (Figure 1). Other EBV$^+$ B cell lines (Daudi, lymphoblastoid cell line [LCL] 1, and LCL-2) were consistently positive for EBER. In addition to B cell lines, NK cell lines (SNK-1, SNK-6, SNK-10, and KAI3) and EBV$^+$ T cell lines (SNT-13 and SNT-16) were also positive for EBER, whereas EBV$^-$ B cell (BJAB), NK cell (KHYG-1), and T cell (MOLT-4 and Jurkat) lines were negative for EBER.

Dual staining for surface antigens and EBER. To identify and characterize EBV-infected cells, surface lymphocyte antigens and nuclear EBER must be detected simultaneously. To this end, we first stained surface antigens with PE- or PC5-labeled monoclonal antibodies and then fixed and hybridized the cells with the EBER PNA probe. After enhancement of fluorescence intensity with Alexa Fluor 488 antibodies, both Alexa Fluor 488–labeled EBER and PE- or PC5-labeled surface antigens were detected by flow cytometry. As shown in Figure 2, the EBV$^+$ B cell line, Raji, was positive for Alexa Fluor 488–labeled EBER, PE-labeled CD19, and PC5-labeled HLA-DR, but negative for CD2, CD3, CD16, and CD56. In contrast, the EBV$^+$ NK cell line, SNK-6, was positive for EBER, CD2, CD56, and HLA-DR, but negative for CD3 and CD19. The EBV$^+$ T cell line, SNT-13, was positive for EBER, CD2, and CD3, but negative for CD16, CD19, CD56, and HLA-DR. The EBV$^-$ cell line BJAB was negative for EBER, but surface CD19 and HLA-DR antigens were detected (Figure 2).

The dual staining for surface antigens and EBER was further confirmed by confocal microscopy (Figure 3). PE-labeled CD19 and PC5-labeled HLA-DR were present on the surface of both Raji and BJAB cells, whereas Alexa Fluor 488–labeled EBER was specifically detected in the nucleus of Raji cells but not BJAB cells. In contrast, CD3 and CD2 were not present on the surface of Raji cells but were detected on the surface of the EBV$^+$ T cell line, SNT-13.

Sensitivity of the FISH assay in identifying EBV$^+$ cells. To determine the lower detection limit of the FISH assay for EBV$^+$ cells, we mixed EBV$^+$ Raji and EBV$^-$ BJAB cells in various ratios and analyzed them using the FISH assay (Figure 4). When 10% of Raji cells were mixed with 90% of BJAB cells, 8.9% of CD19$^+$EBER$^+$ cells could be separated from CD19$^+$EBER$^-$ cells using the FISH assay. Consistently, as the Raji/BJAB ratio decreased, the percentage of CD19$^+$EBER$^+$ cells also decreased. EBER$^+$ cells could be quantified down to a ratio of 1:10,000 (Raji, 0.01%, CD19$^+$EBER$^+$ cells, 0.013%), although the population of CD19$^+$EBER$^+$ cells was not so clear at this ratio. When 0.001% of Raji cells were mixed with BJAB cells, the percentage of CD19$^+$EBER$^+$ cells was almost equal to 100% of

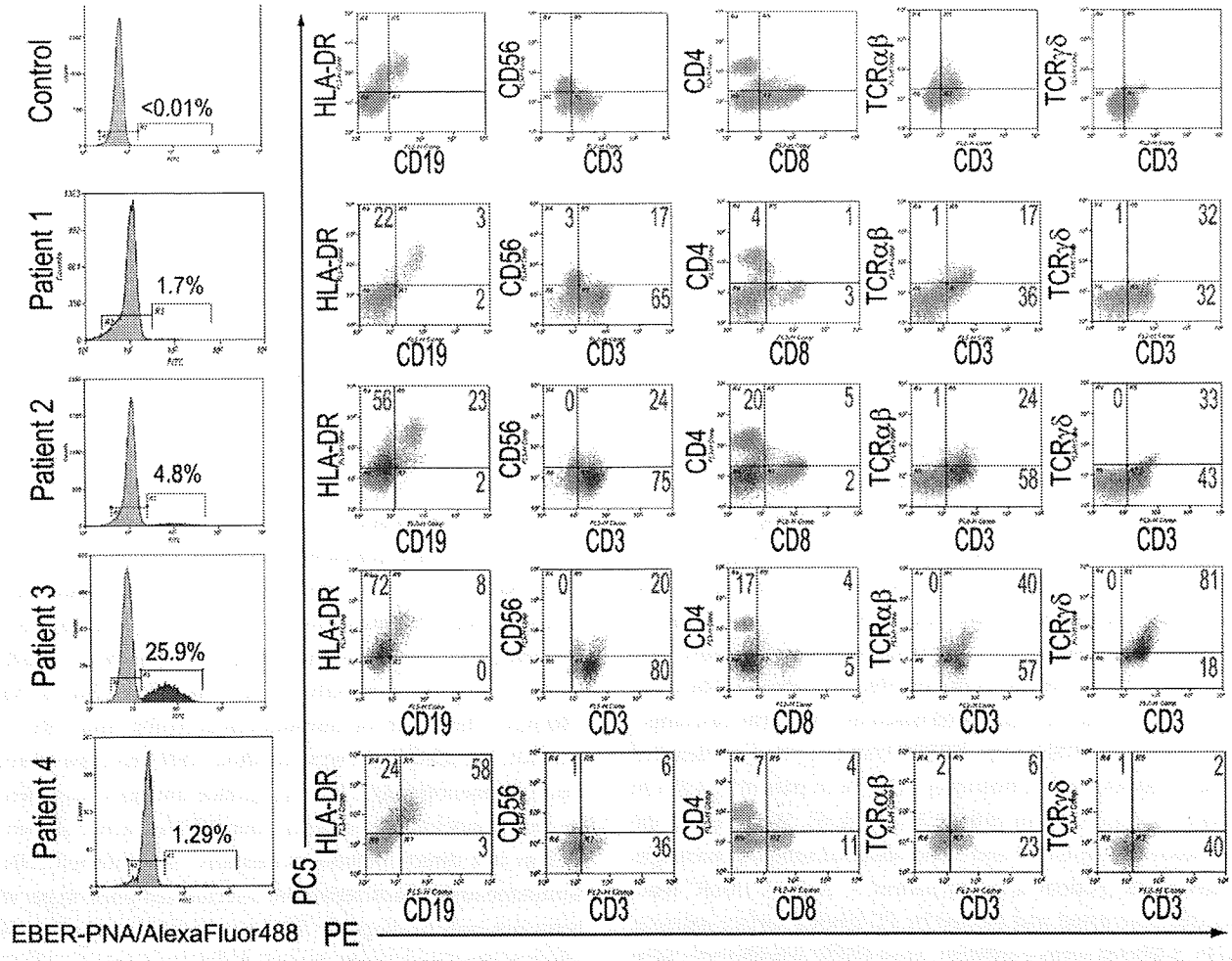

Figure 6. Quantification and identification of Epstein-Barr virus (EBV)–infected lymphocytes in patients with EBV-related lymphoproliferative diseases by flow cytometric in situ hybridization assay. Peripheral blood mononuclear cells were stained with phycoerythrin (PE)–labeled or PE–cyanin 5 (PC5)–labeled monoclonal antibodies and then fixed, permeabilized, and hybridized with the EBV-encoded small RNA (EBER) peptide nucleic acid (PNA) probe. After enhancement of fluorescent signals, the cells were analyzed by flow cytometry. Numbers in histograms represent percentages of $EBER^+$ lymphocytes in the total lymphocyte population. $EBER^+$ lymphocytes *(red)* and $EBER^-$ lymphocytes *(gray)* were gated and plotted on quadrants as PE-labeled and PC5-labeled surface antigens. Numbers in quadrants indicate percentages of $EBER^+$ cells for each surface immunophenotype. A healthy EBV-seropositive donor served as the control; patients 1–3 had hydroa vacciniforme–like EBV-associated T lymphoproliferative disease, and patient 4 had posttransplantation B cell lymphoproliferative disease. FITC, fluorescein isothiocyanate; TCR, T cell receptor.

BJAB cells (0.003% vs 0.003%), suggesting that the FISH assay was not quantitative at these ratios.

To confirm the accuracy and reproducibility of the FISH assay, we performed the mixing experiments (Raji, EBV^+ B cell line; BJAB, EBV^- B cell line) 2 more times and additional mixing experiments (SNT13, EBV^+ T cell line; Jurkat, EBV^- T cell line) in triplicate. The resulting correlations between the percentage of $EBER^+$ cells observed by FISH and the percentage of actual input EBV^+ cells are shown in Figure 5. These data show a clear correlation at 0.1%–10%, indicating that the assay was able to detect $\geq$0.1% of the EBV^+ cells accurately and reproducibly.

Application of the FISH assay to human PBMCs. PBMCs were obtained from 5 healthy volunteer donors and analyzed using the FISH assay. All donors were seropositive for EBV, but EBV DNA was not detected in their PBMCs by real-time PCR. Using the FISH assay, $EBER^+$ cells were not detected in any of the donors, whereas the positive control PNA probe directed against glyceralaldehyde 3-phosphate dehydrogenase was positive for all PBMCs (data not shown). Dual staining with antibodies to surface antigens and PNA probes showed that most lymphocyte markers were successfully detected and that distinct lymphocyte subsets could be separated, although some surface antigen intensities were not sufficient to separate certain populations (eg, CD56 and TCR$\alpha\beta$). A representative result is shown in Figure 6 (control).

Next, we applied the FISH assay to 3 patients with hydroa vacciniforme–like lymphoproliferative disease. These patients

Table 1. Clinical and Virologic Characteristics of Patients with Epstein-Barr Virus (EBV)–Associated Lymphoproliferative Diseases

Patient	Sex	Age, years	Age at onset, years	Diagnosis	EBV clonality	TCR gene rearrangement	EBV DNA, copies/μg DNA						EBV DNA, copies/mL whole blood
							PBMCs	$CD3^+$	$TCR\alpha\beta^+$	$TCR\gamma\delta^+$	$CD19^+$	$CD3^-CD56^+$	
1	M	16	5	Hydroa vacciniforme	Monoclonal	Vγlf,Vγ10/Jγ,Vδ/Jδ	6100	16,380	8310	101,210	ND	860	11,850
2	M	11	5	Hydroa vacciniforme	Monoclonal	Vγlf,Vγ10/Jγ,Vδ/Jδ	10,040	13,230	210	87,420	ND	240	ND
3	M	6	3	Hydroa vacciniforme	Monoclonal	Vδ/Jδ	41,760	46,730	6400	190,100	9090	6400	ND
4	M	6	6	PTLD	ND	ND	22,020	920	ND	ND	91,990	7290	47,660

NOTE. ND, not done; PBMCs, peripheral blood mononuclear cells; PTLD, posttransplantation lymphoproliferative disease; TCR, T cell receptor.

had no symptoms aside from photosensitivity and papulovesicular eruptions on their faces or arms. Skin biopsies were performed in patients 1 and 3. Small lymphoid cells without marked atypia infiltrated both the dermis and epidermis and were positive for EBER. These findings were compatible with hydroa vacciniforme–like lymphoproliferative disease, according to the World Health Organization classification [6]. The infiltrating cells were $CD3^+$ but $CD56^-$, indicating that they were T cells; further immunophenotyping for $TCR\alpha\beta$ and $TCR\gamma\delta$ was not performed. Extremely high amounts of EBV DNA with monoclonality were detected in the 3 patients' peripheral blood (Table 1). The clonality of the T cells was confirmed based on TCR gene rearrangement. Using the FISH assay, $EBER^+$ lymphocytes were detected in their PBMCs, with a frequency of 1.7% in patient 1, 4.8% in patient 2, and 25.9% in patient 3 (Figure 6). We repeated the FISH assay for patients 2 and 3 and obtained similar percentages of EBV^+ cells (patient 2, 5.0%; patient 3, 20.7%). $EBER^+$ lymphocytes were gated and plotted by PE-labeled surface antigens and PC5-labeled surface antigens. Most $EBER^+$ lymphocytes were $CD3^+CD4^-CD8^-TCR\gamma\delta^+$ T cells in the 3 patients examined. HLA-DR was expressed in $EBER^+$ lymphocytes from patients 2 and 3. To confirm these results, we applied an immunobead method to sort PBMCs into $CD3^+$, $TCR\alpha\beta^+$, $TCR\gamma\delta^+$, $CD19^+$, and $CD3^-CD56^+$ fractions and used quantitative real-time PCR to quantify EBV DNA in each fraction. The quantity of EBV DNA was high in the $CD3^+$ and $TCR\gamma\delta^+$ fractions but not in the $CD19^+$, $CD3^-CD56^+$, or $TCR\alpha\beta^+$ fractions (Table 1). For comparison, PBMCs from a patient with posttransplantation B cell lymphoproliferative disease were analyzed by both the FISH assay (Figure 6) and immunobead sorting, followed by EBV DNA quantification (Table 1). Both assays indicated that B cells in the peripheral blood of the patient were EBV^+, confirming the reliability of the FISH assay.

DISCUSSION

In this study, we established a novel FISH assay to directly quantify and simultaneously characterize EBV-infected lymphocytes using a commercially available EBER PNA probe. The probe is currently used to detect EBV-infected cells in formalin-fixed, paraffin-embedded tissue specimens. Just et al [16] also used this probe in a FISH assay. Crouch et al [30] used oligonucleotide probes directed against EBER in a FISH assay and succeeded in simultaneously detecting both EBER and surface antigens. However, both of these studies used FISH assays only with cell lines, and subsequent application to human PBMCs has not been reported. We preliminarily tested the EBER PNA probe with clinical specimens, but the fluorescence intensity of the probe was not sufficient to separate EBV^+ peripheral blood cells from EBV^- cells (data not shown). By enhancing fluorescence and photostability and modifying the fixation and hybridization steps, we successfully stained both EBER and surface antigens, not only in cell lines but also in human PBMCs. The order of immunophenotyping and ISH is important. We tried the reverse method (ISH preceded by surface immunophenotyping), but no surface antigens were detected by the monoclonal antibodies after ISH (data not shown).

This is a direct method to quantify EBV-infected cells and simultaneously characterize the infected cell phenotype, which helps not only to diagnose EBV-associated diseases but also to select monoclonal antibody–based therapy, such as anti-CD20 (rituximab) or anti-CD52 (Campath-1). We stained only surface lymphocyte markers in this study, but additional surface or intracellular molecules, such as cell adhesion markers, cytotoxic granules, or cytokines, will enable us to characterize and examine the function of EBV-infected lymphocytes. Furthermore, this method can be applied not only to peripheral blood but also to bone marrow and other body fluids, such as ascites, pleural effusions, and cerebrospinal fluid. In addition, FISH can be used for flow cytometric sorting of $EBER^+$ cells, which will further expand the ability to isolate and extensively study EBV-infected lymphocytes.

As a noninvasive method to diagnose and monitor EBV-associated lymphoproliferative diseases, measuring viral load in the peripheral blood is a necessary clinical tool. Quantitative PCR assays, such as real-time PCR, are the easiest and most reliable way to measure EBV load and are widely used for diagnosing and managing EBV-associated lymphoproliferative diseases, such as posttransplantation lymphoproliferative disease [7, 31–33]. The FISH assay has some disadvantages compared with quantitative PCR. First, the FISH assay has a lower sensitivity, although it can detect ≥0.1% of EBV-infected cells. Second, this assay cannot be applied to EBV-associated diseases

in which EBV-infected cells do not migrate into the peripheral blood, such as nasopharyngeal carcinoma or Hodgkin lymphoma [7, 34, 35]. Another unresolved problem with this assay is that after hybridization, the fluorescent signals of some surface antigens and antibodies were weak and cell separation was incomplete (eg, CD56 and TCR$\alpha\beta$ in Figure 6). We have not clarified this phenomenon completely, but we believe that antigen-antibody complexes were degraded or detached under the harsh hybridization conditions. The extent of this decrease in fluorescent signals differed among antibodies. We screened several monoclonal antibodies with different fluorochromes from different manufacturers for each surface antigen and then selected the best antibodies, as listed in Methods. Thus, selecting the appropriate antibody is important when performing the FISH assay. This problem may be overcome by using better antibodies, cross-linking antibodies or biotin-avidin enhancement, or modifying the fixation or hybridization steps, but the combination of antibodies and the hybridization conditions used in this study are sufficient to separate B, T, and NK cells from other populations.

Hydroa vacciniforme–like lymphoproliferative disease is an EBV$^+$ cutaneous malignancy associated with photosensitivity [6]. Although this condition is rare, it affects children and adolescents from Asia and Latin America [36–39]. It is characterized by a papulovesicular eruption that generally proceeds to ulceration and scarring. In some cases, systemic symptoms may be present, including fever, wasting, lymphadenopathy, and hepatosplenomegaly. In hydroa vacciniforme–like eruption, T cells with cytotoxic molecules often infiltrate the superficial dermis and subcutaneous tissues [39]. Most persons with this condition have clonal rearrangement of the TCR genes. EBV in these patients is also monoclonal, as shown terminal repeat analysis. These results indicate that clonal expansion of EBV-infected T cells causes the disease. However, the reported phenotypes of these T cells are variable, and both CD4$^+$ and CD8$^+$ T cell subsets have been reported [37, 40]. Most studies lack direct confirmation of these cell populations by double-staining with EBER and surface antigens.

In 3 patients with hydroa vacciniforme–like lymphoproliferative disease, we demonstrated that 1.7%–25.9% of peripheral lymphocytes were EBER$^+$ and that these lymphocytes were primarily CD3$^+$CD4$^-$CD8$^-$TCR$\gamma\delta^+$ T cells. This is the first study to determine the precise phenotype of EBV-infected lymphocytes in hydroa vacciniforme–like lymphoproliferative disease. $\gamma\delta$ T cells are the major T cell population in the epithelium of the skin and mucosa. They secrete various cytokines and have cytolytic properties [41]. It is possible that EBV-infected $\gamma\delta$ T cells play a central role in the formation of hydroa vacciniforme–like eruptions. The 3 patients examined in this study had no symptoms other than eruptions for several years (3–11 years), although they had a high percentage of clonal, EBV-infected lymphocytes in their peripheral blood. The prognosis of hydroa vacciniforme–like lymphoproliferative disease has been reported to be variable, and some cases do not progress for up to 10–15 years or seem to spontaneously enter remission [39, 42]. The 3 patients in our study may be exceptional and may not be representative of this patient population. Further investigation with a larger number of patients is needed to conclude that $\gamma\delta$ T cells are the primary EBV-infected cells in hydroa vacciniforme–like lymphoproliferative disease.

Hydroa vacciniforme–like eruption is also seen in severe chronic active EBV infection, which is caused by the clonal expansion of EBV-infected T or NK cells and seen mainly in East Asia [42–45]. These 2 conditions overlap, but their definitions are unclear [6, 46]. Because the 3 patients in the present study had only skin-restricted symptoms, they did not fulfil the classic criteria for chronic active EBV infection [47]. However, both severe chronic active EBV infection and hydroa vacciniforme–like lymphoproliferative disease develop in children and young adults from East Asia and may be caused by the clonal expansion of EBV-infected T or NK cells. To define and differentiate these diseases, additional data on EBV-associated lymphoproliferative diseases are needed. The FISH assay described in this study is a noninvasive, direct, and relatively convenient method to identify and characterize EBV-infected lymphocytes. With this novel method, we hope to further clarify the pathogenesis of EBV-associated lymphoproliferative diseases, including chronic active EBV infection, and to classify each disease more accurately.

Acknowledgments

We thank Tatsuya Tsurumi (Aichi Cancer Center) for the Raji and Daudi cell lines, Akihiro Tomita (Nagoya University Graduate School of Medicine) for the MOLT-4 and Jurkat cell lines, and Norio Shimizu (Tokyo Medical and Dental University) and Ayako Demachi-Okamura (Aichi Cancer Center) for the SNK-1, -6, and -10 and the SNT-13 and -16 cell lines. KAI3 and KHYG-1 were obtained from the Japanese Collection of Research Bioresources. We also thank Tom Just (Dako) for providing valuable comments regarding the FISH assay.

References

1. Straus SE, Cohen JI, Tosato G, Meier J. NIH conference. Epstein-Barr virus infections: biology, pathogenesis, and management. Ann Intern Med **1993**; 118:45–58.
2. Cohen JI. Epstein-Barr virus infection. N Engl J Med **2000**; 343:481–92.
3. Williams H, Crawford DH. Epstein-Barr virus: the impact of scientific advances on clinical practice. Blood **2006**; 107:862–9.
4. Rickinson AB, Kieff E. Epstein-Barr virus and its replication. In: Knipe DM, Howly PM, eds. Virology. 5th ed. Vol. 2. Philadelphia: Wolters Kluwer/Lippincott Williams & Wilkins, **2006**:2603–54.
5. Rickinson AB, Kieff E. Epstein-Barr virus. In: Knipe DM, Howly PM, eds. Virology. 5th ed. Vol. 2. Philadelphia: Wolters Kluwer/Lippincott Williams & Wilkins, **2006**:2655–700.
6. Quintanilla-Martinez L, Kimura H, Jaffe ES. EBV+ T-cell lymphoma of childhood. In: Swerdlow SH, Campo E, Harris NL, et al, eds. WHO

classification of tumours of haematopoietic and lymphoid tissues. 4th ed. Lyon: WHO Press, **2008**:278–80.
7. Kimura H, Ito Y, Suzuki R, Nishiyama Y. Measuring Epstein-Barr virus (EBV) load: the significance and application for each EBV-associated disease. Rev Med Virol **2008**; 18:305–19.
8. Randhawa PS, Jaffe R, Demetris AJ, et al. Expression of Epstein-Barr virus-encoded small RNA (by the EBER-1 gene) in liver specimens from transplant recipients with post-transplantation lymphoproliferative disease. N Engl J Med **1992**; 327:1710–4.
9. Middeldorp JM, Brink AA, van den Brule AJ, Meijer CJ. Pathogenic roles for Epstein-Barr virus (EBV) gene products in EBV-associated proliferative disorders. Crit Rev Oncol Hematol **2003**; 45:1–36.
10. Nielsen PE, Egholm M, Berg RH, Buchardt O. Sequence-selective recognition of DNA by strand displacement with a thymine-substituted polyamide. Science **1991**; 254:1497–500.
11. Egholm M, Buchardt O, Christensen L, et al. PNA hybridizes to complementary oligonucleotides obeying the Watson-Crick hydrogen-bonding rules. Nature **1993**; 365:566–8.
12. Demidov VV, Potaman VN, Frank-Kamenetskii MD, et al. Stability of peptide nucleic acids in human serum and cellular extracts. Biochem Pharmacol **1994**; 48:1310–3.
13. Lansdorp PM, Verwoerd NP, van de Rijke FM, et al. Heterogeneity in telomere length of human chromosomes. Hum Mol Genet **1996**; 5: 685–91.
14. Zijlmans JM, Martens UM, Poon SS, et al. Telomeres in the mouse have large inter-chromosomal variations in the number of T2AG3 repeats. Proc Natl Acad Sci USA **1997**; 94:7423–8.
15. Lansdorp PM. Telomeres, stem cells, and hematology. Blood **2008**; 111: 1759–66.
16. Just T, Burgwald H, Broe MK. Flow cytometric detection of EBV (EBER snRNA) using peptide nucleic acid probes. J Virol Methods **1998**; 73: 163–74.
17. Iwatsuki K, Xu Z, Takata M, et al. The association of latent Epstein-Barr virus infection with hydroa vacciniforme. Br J Dermatol **1999**; 140:715–21.
18. Nava VE, Jaffe ES. The pathology of NK-cell lymphomas and leukemias. Adv Anat Pathol **2005**; 12:27–34.
19. Zhang Y, Nagata H, Ikeuchi T, et al. Common cytological and cytogenetic features of Epstein-Barr virus (EBV)-positive natural killer (NK) cells and cell lines derived from patients with nasal T/NK-cell lymphomas, chronic active EBV infection and hydroa vacciniforme-like eruptions. Br J Haematol **2003**; 121:805–14.
20. Tsuge I, Morishima T, Morita M, Kimura H, Kuzushima K, Matsuoka H. Characterization of Epstein-Barr virus (EBV)-infected natural killer (NK) cell proliferation in patients with severe mosquito allergy: establishment of an IL-2-dependent NK-like cell line. Clin Exp Immunol **1999**; 115:385–92.
21. Sahai Srivastava BI, Minowada J. Terminal deoxynucleotidyl transferase activity in a cell line (molt-4) derived from the peripheral blood of a patient with acute lymphoblastic leukemia. Biochem Biophys Res Commun **1973**; 51:529–35.
22. Yagita M, Huang CL, Umehara H, et al. A novel natural killer cell line (KHYG-1) from a patient with aggressive natural killer cell leukemia carrying a p53 point mutation. Leukemia **2000**; 14:922–30.
23. Kuzushima K, Hoshino Y, Fujii K, et al. Rapid determination of Epstein-Barr virus-specific $CD8^+$ T-cell frequencies by flow cytometry. Blood **1999**; 94:3094–100.
24. Yamauchi Y, Kiriyama K, Kubota N, Kimura H, Usukura J, Nishiyama Y. The UL14 tegument protein of herpes simplex virus type 1 is required for efficient nuclear transport of the alpha transinducing factor VP16 and viral capsids. J Virol **2008**; 82:1094–106.
25. Kimura H, Morita M, Yabuta Y, et al. Quantitative analysis of Epstein-Barr virus load by using a real-time PCR assay. J Clin Microbiol **1999**; 37:132–6.
26. Kimura H, Hoshino Y, Hara S, et al. Differences between T cell-type and natural killer cell-type chronic active Epstein-Barr virus infection. J Infect Dis **2005**; 191:531–9.
27. Kimura H, Hoshino Y, Kanegane H, et al. Clinical and virologic characteristics of chronic active Epstein-Barr virus infection. Blood **2001**; 98:280–6.
28. van Dongen JJ, Langerak AW, Bruggemann M, et al. Design and standardization of PCR primers and protocols for detection of clonal immunoglobulin and T-cell receptor gene recombinations in suspect lymphoproliferations: report of the BIOMED-2 Concerted Action BMH4-CT98–3936. Leukemia **2003**;17:2257–317.
29. Sandberg Y, van Gastel-Mol EJ, Verhaaf B, Lam KH, van Dongen JJ, Langerak AW. BIOMED-2 multiplex immunoglobulin/T-cell receptor polymerase chain reaction protocols can reliably replace Southern blot analysis in routine clonality diagnostics. J Mol Diagn **2005**; 7:495–503.
30. Crouch J, Leitenberg D, Smith BR, Howe JG. Epstein-Barr virus suspension cell assay using in situ hybridization and flow cytometry. Cytometry **1997**; 29:50–7.
31. Rooney CM, Loftin SK, Holladay MS, Brenner MK, Krance RA, Heslop HE. Early identification of Epstein-Barr virus-associated post-transplantation lymphoproliferative disease. Br J Haematol **1995**; 89:98–103.
32. Rowe DT, Webber S, Schauer EM, Reyes J, Green M. Epstein-Barr virus load monitoring: its role in the prevention and management of post-transplant lymphoproliferative disease. Transpl Infect Dis **2001**; 3:79–87.
33. Niesters HG. Molecular and diagnostic clinical virology in real time. Clin Microbiol Infect **2004**; 10:5–11.
34. Ambinder RF, Lin L. Mononucleosis in the laboratory. J Infect Dis **2005**; 192:1503–4.
35. Chan KC, Zhang J, Chan AT, et al. Molecular characterization of circulating EBV DNA in the plasma of nasopharyngeal carcinoma and lymphoma patients. Cancer Res **2003**; 63:2028–32.
36. Barrionuevo C, Anderson VM, Zevallos-Giampietri E, et al. Hydroa-like cutaneous T-cell lymphoma: a clinicopathologic and molecular genetic study of 16 pediatric cases from Peru. Appl Immunohistochem Mol Morphol **2002**; 10:7–14.
37. Chen HH, Hsiao CH, Chiu HC. Hydroa vacciniforme-like primary cutaneous CD8-positive T-cell lymphoma. Br J Dermatol **2002**; 147: 587–91.
38. Cho KH, Lee SH, Kim CW, et al. Epstein-Barr virus-associated lymphoproliferative lesions presenting as a hydroa vacciniforme-like eruption: an analysis of six cases. Br J Dermatol **2004**; 151:372–80.
39. Iwatsuki K, Satoh M, Yamamoto T, et al. Pathogenic link between hydroa vacciniforme and Epstein-Barr virus-associated hematologic disorders. Arch Dermatol **2006**; 142:587–95.
40. Doeden K, Molina-Kirsch H, Perez E, Warnke R, Sundram U. Hydroa-like lymphoma with CD56 expression. J Cutan Pathol **2008**; 35:488–94.
41. Kaufmann SH. gamma/delta and other unconventional T lymphocytes: what do they see and what do they do? Proc Natl Acad Sci U S A **1996**; 93:2272–9.
42. Nitta Y, Iwatsuki K, Kimura H, et al. Fatal natural killer cell lymphoma arising in a patient with a crop of Epstein-Barr virus-associated disorders. Eur J Dermatol **2005**; 15:503–6.
43. Kanegane H, Nomura K, Miyawaki T, Tosato G. Biological aspects of Epstein-Barr virus (EBV)-infected lymphocytes in chronic active EBV infection and associated malignancies. Crit Rev Oncol Hematol **2002**; 44:239–49.
44. Kimura H, Morishima T, Kanegane H, et al. Prognostic factors for chronic active Epstein-Barr virus infection. J Infect Dis **2003**; 187:527–33.
45. Katagiri Y, Mitsuhashi Y, Kondo S, Kanazawa C, Iwatsuki K, Tsunoda T. Hydroa vacciniforme-like eruptions in a patient with chronic active EB virus infection. J Dermatol **2003**; 30:400–4.
46. Ohshima K, Kimura H, Yoshino T, et al. Proposed categorization of pathological states of EBV-associated T/natural killer-cell lymphoproliferative disorder (LPD) in children and young adults: overlap with chronic active EBV infection and infantile fulminant EBV T-LPD. Pathol Int **2008**; 58:209–17.
47. Straus SE. The chronic mononucleosis syndrome. J Infect Dis **1988**; 157:405–12.

ELSEVIER

Experimental Hematology

Experimental Hematology 2009;37:1393–1399

Downregulation of *GATA-2* and overexpression of adipogenic gene-PPARγ in mesenchymal stem cells from patients with aplastic anemia

Yinyan Xu[a], Yoshiyuki Takahashi[a], Yue Wang[a,b], Asahito Hama[a], Nobuhiro Nishio[a], Hideki Muramatsu[a], Makito Tanaka[a], Nao Yoshida[a], Itzel Bustos Villalobos[a], Hiroshi Yagasaki[a], and Seiji Kojima[a]

[a]*Department of Pediatrics, Nagoya University Graduate School of Medicine, Nagoya, Japan;* [b]*Department of Pediatrics, the First Hospital of Jilin University, Changchun, Jilin, China*

(Received 25 March 2009; revised 12 September 2009; accepted 17 September 2009)

Aplastic anemia (AA) is characterized by a reduced number of hematopoietic stem cells and fatty replacement in the bone marrow. Transcriptional factor *GATA-2* plays several important roles in both hematopoiesis and adipogenesis. Decreased levels of *GATA-2* compromise the proliferation and survival of hematopoietic stem cells. *GATA-2* suppresses adipocyte differentiation through direct inhibition of adipogenic factors, including peroxisome proliferator-activated receptor−γ *(PPARγ)*. Previous studies have shown that expression of *GATA-2* is decreased in marrow CD34-positive cells in AA. To elucidate the mechanisms of fatty marrow replacement, we evaluated the mRNA expression for *GATA-2* and *PPARγ* in mesenchymal stem cells (MSCs) from patients with AA by quantitative real-time polymerase chain reaction. *GATA-2* expression by MSCs from AA patients was significantly lower than in normal subjects. Conversely, expression of *PPARγ* was significantly higher in AA patients. Western blot analysis demonstrated that protein levels of *GATA-2* were lower in AA patients than those in normal subjects. Moreover, incubation with interferon-γ induced downregulation of *GATA-2* levels in MSCs from normal subjects. These findings indicate that fatty marrow replacement in AA patients can be explained by downregulation of *GATA-2* and overexpression of *PPARγ* in MSCs. Decreased expression of *GATA-2* might be responsible for the pathogenesis and development of the clinical features of the disease. © 2009 ISEH - Society for Hematology and Stem Cells. **Published by Elsevier Inc.**

Aplastic anemia (AA) is characterized by a reduced number of hematopoietic stem cells (HSCs) and fatty replacement in bone marrow (BM), resulting in pancytopenia. To date, most efforts by investigators have concentrated on the elucidation of immune-mediated mechanisms of hematopoietic cell destruction [1–3]. Although replacement of hematopoietically active marrow with fat cells is another characteristic feature of AA, the fat cells themselves have received little attention, and the mechanisms of fatty marrow replacement remain unclear.

The transcription factor *GATA-2* is expressed in HSCs and early progenitors and plays a critical role in hematopoiesis [4]. Decreased levels of *GATA-2* compromise proliferation and survival of HSCs [5,6]. Considering the critical role of *GATA-2* in hematopoiesis, Fujimaki et al. quantified the levels of mRNA of *GATA-2*, which were markedly lower in AA patients when compared with normal subjects [7]. GeneChip analysis also confirmed that *GATA-2* gene expression was downregulated in CD34-positive marrow cells from AA patients [8]. These findings suggest that aberrant expression of *GATA-2* is responsible for the pathogenesis of AA.

Adipocytes are differentiated from preadipocytes, which are thought to emerge from multipotent mesenchymal stem cells (MSCs) [9]. *GATA-2* is specifically expressed in not only hematopoietic tissues, but also preadipocytes, and is known to be an important adipogenic regulator. Preadipocytes are the main components of the BM microenvironment and *GATA-2* suppresses adipocyte differentiation, keeping the cells at the preadipocyte stage. Suppression of adipocyte differentiation by *GATA-2* is mediated through

Offprint requests to: Seiji Kojima, M.D., Ph.D., Department of Pediatrics, Nagoya University Graduate School of Medicine, 65 Tsurumai-cho, Showa-ku, Nagoya 466-8550, Japan; E-mail: kojimas@med.nagoya-u.ac.jp

0301-472X/09 $–see front matter.
doi: 10.1016/j.exphem.2009.09.005

direct inhibition of adipogenic transcriptional factors, including peroxisome proliferator-activated receptor−γ (*PPARγ*) [10]. *PPARγ* has been shown to be expressed in both preadipocytes and MSCs [11]. These observations prompted us to investigate *GATA-2* and *PPARγ* mRNA expression in MSCs derived from AA patients. We show here that *GATA-2* expression by MSCs from AA patients was reduced significantly, while expression of *PPARγ* was significantly elevated in AA patients when compared with normal subjects. Our findings may help to clarify the mechanisms of fatty marrow replacement in AA patients.

Materials and methods

Patients

Thirty-four AA patients and 15 normal subjects were included in the study. Clinical characteristics of these patients are summarized in Table 1. Diagnosis of AA was established by peripheral blood counts and BM findings, and disease severity was classified using international criteria [12]. Patients were screened for Fanconi anemia and paroxysmal nocturnal hemoglobinuria (PNH) by chromosome breakage analysis and flow cytometry using anti-CD55 and anti-CD59 antibodies. Cytogenetic studies were performed to exclude myelodysplastic syndrome. Aplasia was secondary to acute hepatitis in 4 patients and the cause was unknown in 30 patients. Median age at diagnosis was 10 years, ranging from 2 to 21 years. Of the 19 immunosuppressive therapy (IST)–treated patients, 11 responded and were transfusion-independent at the time of study, while the remaining patients were nonresponders.

Generation of MSCs

BM was collected either at the time of diagnosis or after IST with antithymocytoglobulin and cyclosporine. Response criteria were as described previously [13]. Normal BM samples were obtained from 15 allogenic BM transplantation donors ranging in age from 4 to 45 years. The Institutional Review Board of the Nagoya University Graduate School of Medicine approved the study and written informed consent was obtained from patients or their guardians.

Mononuclear cells were isolated from BM samples by Ficoll-Hypaque density gradient centrifugation. A total of 1×10^7 BM mononuclear cells were cultured in MesenCult Basal Medium (Stem Cell Technologies, Vancouver, Canada) supplemented with human mesenchymal stem cell supplements (Stem Cell Technologies) in a T25 tissue culture flask (Falcon, Franklin Lakes, CA, USA), followed by incubation at 37°C and 5% CO_2 in an incubator for 48 hours. Whole medium and nonadherent cells were then removed and replaced with fresh medium until confluence. At the end of the culture period, residual nonadherent cells and medium were removed by washing with phosphate-buffered saline (PBS) before trypsinization. Adherent cells were trypsinized, washed, and expanded to the second generation. Third-generation MSCs were used in all experiments.

Table 1. Clinical characteristics of patients with aplastic anemia

Clinical characteristics	
No. of patients	34
Median age (y) at diagnosis (range)	10 (2 – 21)
Gender: male/female	16/18
Etiology	
Idiopathic	30
Hepatitis	4
Disease severity at diagnosis	
Very severe	7
Severe	19
Nonsevere	8
Treatment at the time of study	
None	15
After IST	
Responder	11
Nonresponder	8
Duration (mos) from diagnosis to the time of study, median (range)	28 (0 – 308)

IST = immunosuppressive therapy.

Characterization of MSC

MSC immunophenotype was determined using a FACSCaliber flow cytometer (Becton Dickinson Biosciences, San Diego, CA, USA). Anti-human CD13-fluorescein isothiocyanate (FITC), anti-human CD14-FITC, anti-human CD44-PE, and anti-human CD45-FITC were purchased from Immunotech (Marseille, France); anti-human CD29-PE, anti-human CD73-PE, anti-human CD90-PE, anti-human CD106-PE, anti-human CD166-PE, and anti-human human leukocyte antigen–D-related FITC were purchased from Becton Dickinson Biosciences. Anti-human CD34-FITC and anti-human CD105-PE were purchased from DAKO (Glostrup, Denmark) and Beckman Coulter (Marseille, France), respectively. After trypsinization, MSCs (1×10^5) were stained with 5 μg each monoclonal antibody for 30 minutes at 4°C. Cells were washed with 1% fetal calf serum containing PBS and resuspended in 300 μL PBS before analysis.

MSCs demonstrated adipocytogenic and osteocytogenic differentiation as follows. For differentiation into adipocytes, MSCs were seeded at 2×10^5/T25 flask in MesenCult Basal Medium supplemented with human adipocytogenic supplements (Stem Cell Technologies). Culture medium was refreshed every 3 days. After 3 weeks, morphological changes were examined under an inverted microscope. Typical adipocytes had lipid droplets and were stained with Oil Red O. For differentiation into osteoblasts, osteogenic supplement (Stem Cell Technologies) was used instead of adipogenic supplement. Cell layers were stained with silver nitrate to detect calcium deposition.

Quantitative real-time polymerase chain reaction (QRT-PCR)

Total RNA was extracted from third-passage MSCs using an RNeasy Mini kit (Qiagen, Valencia, CA, USA) and concentrations of extracted RNA were measured by spectrophotometry. Synthesis of complementary DNA (cDNA) was performed using a Thermoscript RT-PCR system (Invitrogen, San Diego, CA, USA) according to manufacturer's instructions.

QRT-PCR was performed using an ABI Prism 7000 Sequence Detection System (Applied Biosystems, Branchburg, NJ, USA). Ready-made primers and TaqMan probes for *glyceraldehyde phosphate dehydrogenase* (*GAPDH*) (HS99999905_m1), *PPARγ* (Hs00234592_m1), and *GATA-2* [7] were purchased from Applied Biosystems.

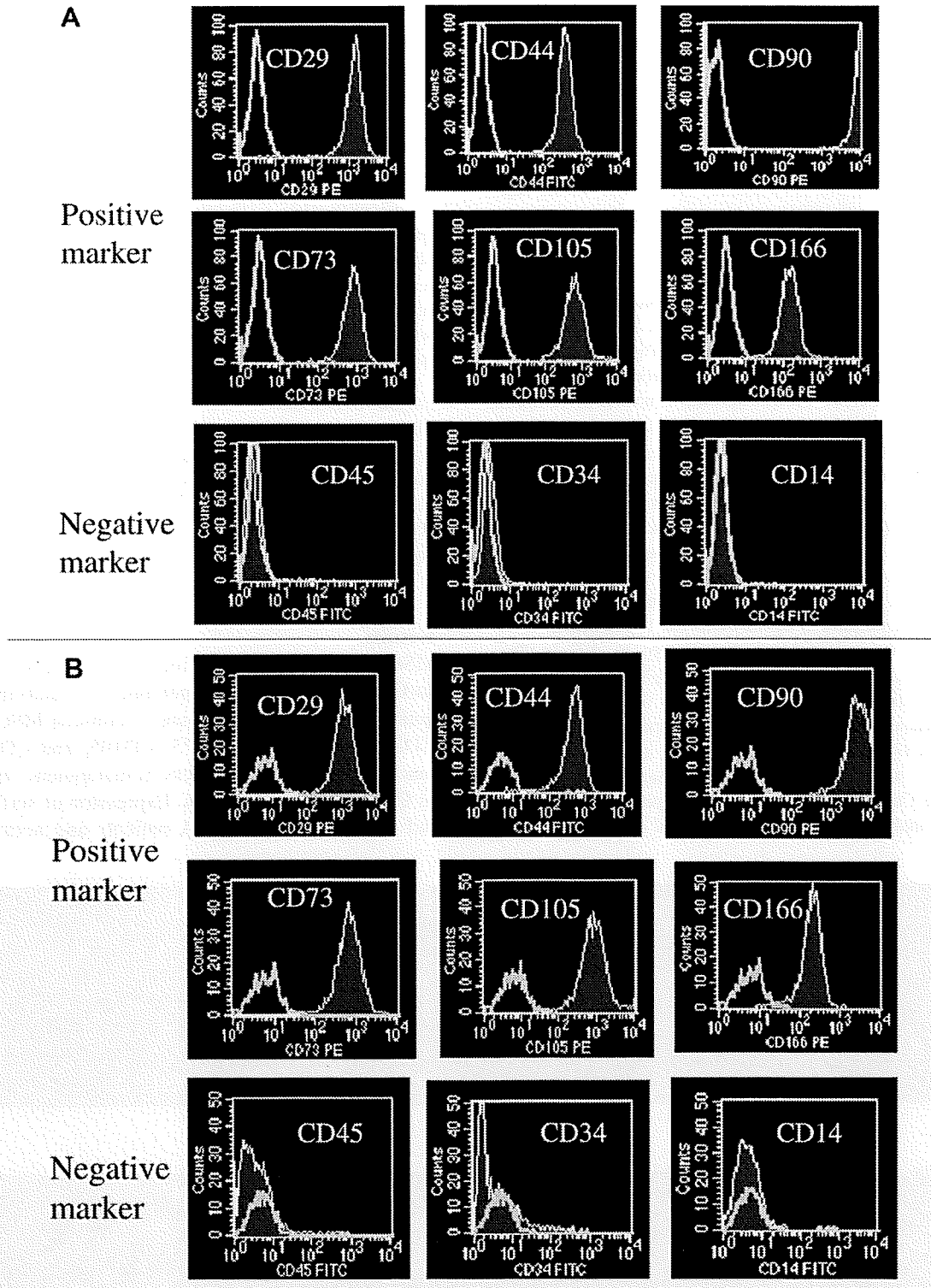

Figure 1. Representative phenotype of mesenchymal stem cells (MSCs) from a normal subject (**A**) and a patient with aplastic anemia (**B**). MSCs express adhesion markers CD29, CD44, CD90, CD73, CD105, and CD166, but not hematological markers CD34, CD45, and CD14. There were no significant differences in the expression of MSC markers between aplastic anemia patients and normal subjects.

PCR was performed in a total volume of 15 μL, containing each fluorogenic probe at 100 nM, each primer at 0.2 μM, 1 × TaqMan Universal PCR Mastermix (Applied Biosystems) and 10 ng sample cDNA or various amounts (0.01, 0.1, 1, 10, or 100 ng) of standard cDNA. Standard RNA was extracted from the K562 cell line for *GATA-2* and MOLM-13 cell line for *PPARγ*. Each test and standard cDNA was amplified in triplicate. PCR conditions were as follows: 2 minutes at 50°C; 10 minutes at

95°C; and 40 cycles consisting of 15 seconds at 95°C and 1 minute at 60°C. Data analysis was performed using ABI Prism sequence detection software (Applied Biosystems). Separate standard curves were generated for the test and reference *GAPDH* genes. Threshold cycle number (Ct) was determined, and the starting gene copy number relative to the reference was determined for each well using a standard curve. Normalized gene expression levels are given as the ratio between the mean value for the target gene and that for the *GAPDH* gene in each sample.

Western blotting

For Western blotting, 5×10^5 MSCs were collected and washed in PBS, and lysed in 100 μL cell lysis buffer for 30 minutes on ice. Cell lysis buffer consisted of 20 mM Tris-HCl (pH 7.5), 150 mM NaCl, 1 mM ethylenediamine tetraacetic acid, 1% Triton X-100, 2.5 mM sodium pyrophosphate, 1 mM β-glycerophosphate, and 1 mM Na_3VO_4 containing a 1:50 dilution of protease inhibitor cocktail. Samples were centrifuged at 14,000*g* for 10 minutes at 4°C, and the supernatants were removed, snap-frozen, and stored at −30°C. After determination of the cell protein concentration using the Bio-Rad protein assay (Bio-Rad, Richmond, CA, USA), 20 μg cell protein samples was resolved by sodium dodecyl sulfate polyacrylamide gel electrophoresis for 60 minutes at 150 V, followed by electrophoretic transfer to nitrocellulose membranes at 0.5 mA/cm^2 for 120 minutes.

Membranes were then blocked overnight at 4°C in Tris-buffered saline containing 0.1% Tween 20 (pH 7.6, TBST) with 5% bovine serum albumin, and were then incubated with the respective primary antibodies at room temperature for 1 hour. Expression of *GATA-2* was analyzed using a rabbit polyclonal anti – *GATA-2* antibody (1:200; sc-9008, Santa Cruz Biotechnology, Santa Cruz, CA, USA). For control purposes, expression of actin was analyzed using a goat polyclonal anti-actin antibody (1:1,000; sc-1615, Vector Laboratories, Burlingame, CA, USA). After washing in TBST, secondary antibodies (anti-rabbit immunoglobulin G or anti-goat immunoglobulin G, 1:2,000; Vector Laboratories) were used to detect specific primary antibodies. Streptavidin-horseradish peroxidase conjugate (1:1,000; Life Technologies, GIBCO BRL, Gaithersburg, MD, USA) was used for detection of secondary antibodies.

Interferon-γ (IFN -γ) in MSC culture

MSCs (8×10^4/well) derived from normal subjects (n = 5) were suspended in six-well culture plates and cultured at 37°C in a 5% CO_2 incubator. At confluence, IFN-γ was added at a dose of 0, 10, 100, or 1,000 IU/mL. After 24 hours, stimulated MSCs were washed, trypsinized, and collected to extract RNA for detection of *GATA-2* expression by real-time PCR.

Statistical analysis

Statview version 5.0 (Abacus Concepts Inc., Berkeley, CA, USA) was used for all statistical analyses. To compare each group of gene expression, Fisher's protected least significant difference was used, and *t*-test was used to compare *GATA-2* expression after IFN-γ stimulation. *P* values <0.05 were defined as indicating significance.

Results

MSCs are typically identified by a combination of cell surface markers and their potential for multilineage differentiation. As shown in Figure 1, cultured MSCs expressed CD29, CD44, CD90, CD73, CD105, and CD166 surface markers, but did not express hematopoietic markers such as CD45, CD34, and CD14. Expression of surface markers did not differ between AA patients and normal subjects.

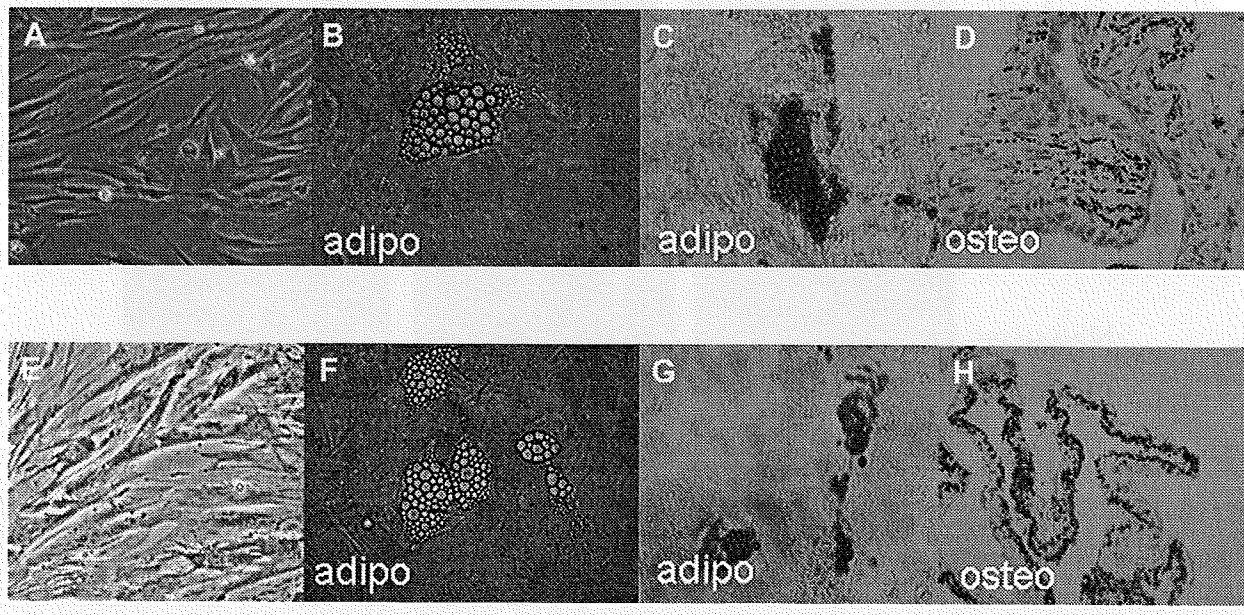

Figure 2. Cultured cells from normal subjects and patients with aplastic anemia were tested for their ability to differentiate. Derived cells from normal subjects (**A** – **D**) and patients (**E** – **H**) were each shown to differentiate into adipogenic (Adipo) and osteogenic (Osteo) lineages. (**A**) and (**E**) show original MSCs; adipogenesis was seen under inverted microscope (**B**,**F**) and Oil Red staining (**C**,**G**). Osteogenesis was indicated by an increase in calcium deposition (**D**,**H**).

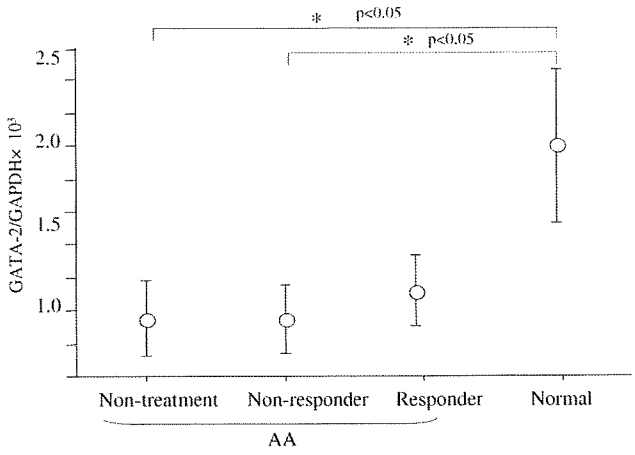

Figure 3. Expression of *GATA-2* in mesenchymal stem cells (MSCs) from aplastic anemia (AA) patients and normal subjects. Expression level was standardized with glyceraldehydes phosphate dehydrogenase (GAPDH) and was shown as a relative ratio. MSCs derived from nontreated patients and immunosuppressive therapy (IST) nonresponders expressed significantly lower amounts of *GATA-2* than normal subjects ($p < 0.05$). On the other hand, IST responder-derived MSCs expressed similar amounts of *GATA-2* when compared with normal subjects.

Cultured MSCs retained their capacity to differentiate into adipogenic and osteogenic lineages (Fig. 2).

GATA-2 expression was measured in third-passage MSCs from AA patients and normal subjects by real-time PCR. *GATA-2* expression levels were found to be significantly different between AA patients and normal subjects (Fig. 3). *GATA-2* levels in MSCs from AA patients before treatment were significantly lower than those in normal subjects ($0.95 \pm 0.23 \times 10^{-3}$ vs $2.00 \pm 0.47 \times 10^{-3}$; $p < 0.05$). Notably, *GATA-2* levels were not significantly different between normal subjects and IST responders ($2.00 \pm 0.47 \times 10^{-3}$ vs $1.12 \pm 0.22 \times 10^{-3}$; $p = 0.07$), while nonresponders had significantly lower *GATA-2* expression levels when compared to normal subjects ($0.95 \pm 0.21 \times 10^{-3}$ vs $2.00 \pm 0.47 \times 10^{-3}$; $p < 0.05$). We also demonstrated that the protein levels of *GATA-2* in MSCs derived from AA patients were lower than those from normal subjects by Western blot analysis (Fig. 4). In nontreated AA patients, both responders and nonresponders to IST, protein levels were lower than those in normal subjects.

Conversely, pretreatment levels of *PPARγ* in MSCs from AA patients were significantly higher than in those from normal subjects ($2.86 \pm 0.84 \times 10^{-2}$ vs $0.95 \pm 0.23 \times 10^{-2}$; $p < 0.05$). Although expression levels of *PPARγ* decreased in response to IST ($1.71 \pm 0.57 \times 10^{-2}$; $p = 0.38$), they remained high in nonresponders ($3.2 \pm 0.68 \times 10^{-2}$; $p < 0.05$) (Fig. 5).

In order to investigate the mechanism of downregulation in *GATA-2* expression, we cultured MSCs derived from normal subjects in the presence of IFN-γ. After IFN-γ stimulation with IFN-γ, *GATA-2* expression was downregulated based on the concentration of IFN-γ (Fig. 6). *GATA-2* expression was $12.37 \pm 0.66 \times 10^{-3}$ in the absence of IFN-γ, and was significantly lower in the presence of 10 IU/mL IFN-γ ($8.96 \pm 0.33 \times 10^{-3}$; $p < 0.05$), 100 IU/mL IFN-γ ($6.53 \pm 0.44 \times 10^{-3}$; $p < 0.01$) and 1,000 IU/mL IFN-γ ($6.03 \pm 0.52 \times 10^{-3}$; $p < 0.01$) when compared with control levels.

Discussion

MSCs isolated from human BM are capable of differentiating into several cell lineages. When cultured in adipogenic medium, MSCs differentiate into adipocytes and accumulate lipid vesicles in the cytoplasm. Because *GATA-2* is a transcriptional factor expressed in HSCs and various other stem cells, we hypothesized that *GATA-2* is also expressed in MSCs isolated from BM. To date, there have been no reports regarding *GATA-2* expression in human MSCs. *GATA-2* serves as a gatekeeper at the onset of adipocyte differentiation and is expressed in preadipocytes, but is downregulated when cells differentiate into mature adipocytes [14]. Preadipocytes are the main components of stromal cells, which form the

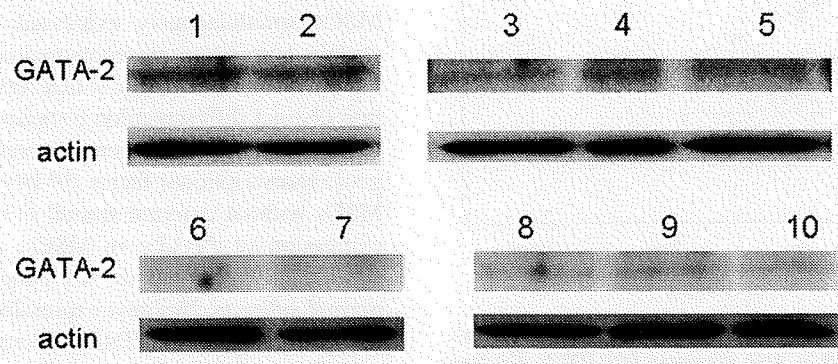

Figure 4. Western blot analysis of *GATA-2* protein in treated or nontreated patients and normal subjects. Whole-cell protein extracts were analyzed using a specific polyclonal anti – *GATA-2* antibody. Upper lanes show *GATA-2* expression; lower lanes show actin expression. Mesenchymal stem cells (MSCs) derived from normal subjects (lanes 1 and 2), nontreated patients (lanes 3, 4, and 5), immunosuppressive therapy (IST) nonresponders (lanes 6 and 7) and IST responders (lanes 8, 9, and 10) were used in Western blotting.

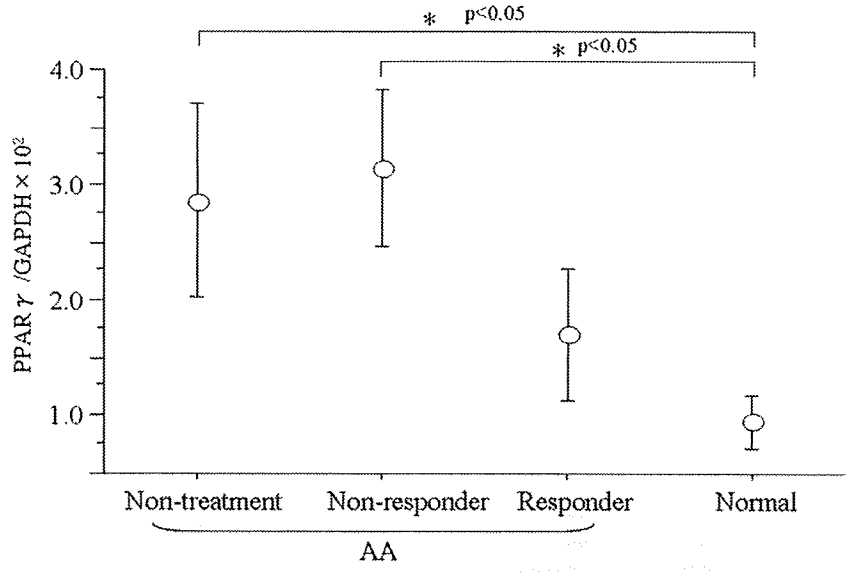

Figure 5. Expression of peroxisome proliferator-activated receptor−γ (*PPARγ*) in mesenchymal stem cells (MSCs) from patients with aplastic anemia (AA) and normal controls. Expression levels were standardized against glyceraldehydes phosphate dehydrogenase (GAPDH) and are shown as relative ratios. *PPARγ* expression of nontreated patients and immunosuppressive therapy (IST) nonresponders was significantly higher when compared with normal subjects ($p < 0.05$). However, in IST responders, *PPARγ* expression did not significantly differ from that in normal subjects.

microenvironment for hematopoiesis in the BM. In this study, we demonstrated that *GATA-2* is expressed in MSCs and that its expression in MSCs is significantly lower in AA patients when compared with normal subjects. *GATA-2* expression in purified CD34-positive cells was also markedly lower in AA patients [7], thus suggesting the presence of a common regulatory mechanism in both HSCs and MSCs.

IFN-γ plays a crucial role in immune-mediated suppression of HSCs in AA. In long-term culture of human BM, in which stromal cells were engineered to constitutively express IFN-γ, the output of long-term culture-initiating cells was markedly diminished, despite low concentrations of IFN-γ in the medium [15]. This implies a pathophysiological role for IFN-γ in the BM microenvironment of AA patients. Okitsu et al. [16] recently discussed the regulation of adipocyte differentiation in BM stromal cells by *GATA-2* using a mouse preadipocyte stromal cell line. The addition of IFN-γ to culture medium significantly suppressed expression of *GATA-2* in the cell line. In addition, they demonstrated that regulatory elements of the *GATA-2* gene in the stromal cell line are the same as those in hematopoietic cells [16]. These findings suggest that a common signal simultaneously suppresses expression of *GATA-2* in both HSCs and MSCs. We also found that when IFN-γ was added to culture medium, *GATA-2* expression of normal MSCs is downregulated.

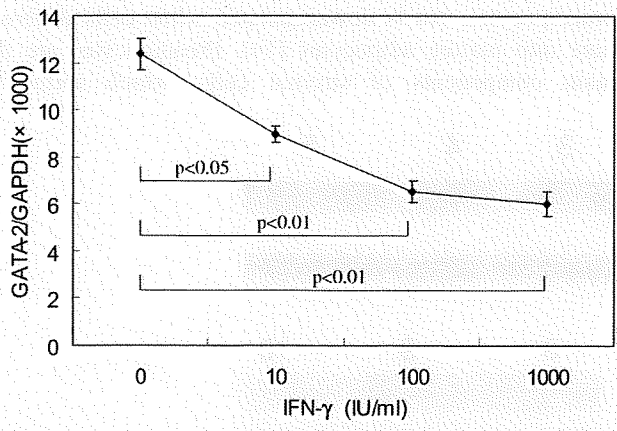

Figure 6. *GATA-2* expression after stimulation with interferon-γ (IFN-γ). Mesenchymal stem cells (MSCs) were stimulated with IFN-γ at various concentrations (0, 10, 100, 1000 IU/mL). In this figure, the relationship between IFN-γ concentration and *GATA-2* expression is shown. When MSCs were stimulated with different concentrations of IFN-γ, *GATA-2* expression was downregulated in a dose-dependent manner.

A single cell-derived colony of undifferentiated human MSCs simultaneously expressed genes characteristic of various committed mesenchymal cell lineages. One explanation for these findings is that MSCs individually entered into distinct differentiation programs, leading to generation of a molecularly heterogeneous population [17]. The adipogenic transcriptional factor *PPARγ* is detectable in human MSCs without external stimuli [11]. We demonstrated the expression of *PPARγ* in MSCs, and its expression was significantly elevated in AA patients when compared to normal subjects. Notably, expression of *GATA-2* increased, while expression of *PPARγ* decreased when patients responded to IST and became transfusion-independent. On the other hand, nonresponders continued to have lower *GATA-2* and higher *PPARγ* expression. This reciprocal expression of *GATA-2* and *PPARγ* is consistent with the

observation that *GATA-2* binds and suppresses the activity of the *PPARγ* promoter.

Taken together with previous reports, these results indicate that the pathological immune response increases levels of IFN-γ in the BM microenvironment, which decreases expression of *GATA-2* in both HSCs and MSCs in AA patients. Decreased *GATA-2* expression in HSCs may compromise hematopoietic function and increased *PPARγ* expression in MSCs may accelerate maturation of preadipocytes, leading to formation of fatty BM.

Acknowledgments

We would like to thank Mr. Miyake for performing Von Kossa staining and Dr. Hiroshi Nagasaki for assistance with Oil red staining for MSC characterization. We would also like to thank Dr. Hideyuki Iwayama and Norishi Ueda for performing Western blot analysis for *GATA-2*.

Conflict of Interest Disclosure

No financial interest/relationships with financial interest relating to the topic of this article have been declared.

References

1. Ascensao J, Pahwa R, Kagan W, Hansen J, Moore M, Good R. Aplastic anaemia: evidence for an immunological mechanism. Lancet. 1976;1:669–671.
2. Bacigalupo A, Valle M, Podesta M, et al. T-cell suppression mediated by mesenchymal stem cells is deficient in patients with severe aplastic anemia. Exp Hematol. 2005;33:819–827.
3. Young NS, Maciejewski J. The pathophysiology of acquired aplastic anemia. N Engl J Med. 1997;336:1365–1372.
4. Tsai FY, Keller G, Kuo FC, et al. An early haematopoietic defect in mice lacking the transcription factor GATA-2. Nature. 1994;371: 221–226.
5. Ling KW, Ottersbach K, van Hamburg JP, et al. GATA-2 plays two functionally distinct roles during the ontogeny of hematopoietic stem cells. J Exp Med. 2004;200:871–882.
6. Rodrigues NP, Janzen V, Forkert R, et al. Haploinsufficiency of GATA-2 perturbs adult hematopoietic stem-cell homeostasis. Blood. 2005;106:477–484.
7. Fujimaki S, Harigae H, Sugawara T, Takasawa N, Sasaki T, Kaku M. Decreased expression of transcription factor GATA-2 in haematopoietic stem cells in patients with aplastic anaemia. Br J Haematol. 2001;113:52–57.
8. Zeng W, Chen G, Kajigaya S, et al. Gene expression profiling in CD34 cells to identify differences between aplastic anemia patients and healthy volunteers. Blood. 2004;103:325–332.
9. Pittenger MF, Mackay AM, Beck SC, et al. Multilineage potential of adult human mesenchymal stem cells. Science. 1999;284:143–147.
10. Tong Q, Tsai J, Hotamisligil GS. GATA transcription factors and fat cell formation. Drug News Perspect. 2003;16:585–588.
11. Janderova L, McNeil M, Murrell AN, Mynatt RL, Smith SR. Human mesenchymal stem cells as an in vitro model for human adipogenesis. Obes Res. 2003;11:65–74.
12. Camitta BM, Thomas ED, Nathan DG, et al. A prospective study of androgens and bone marrow transplantation for treatment of severe aplastic anemia. Blood. 1979;53:504–514.
13. Kojima S, Matsuyama T, Kodera Y. Hematopoietic growth factors released by marrow stromal cells from patients with aplastic anemia. Blood. 1992;79:2256–2261.
14. Tong Q, Dalgin G, Xu H, et al. Function of GATA transcription factors in preadipocyte-adipocyte transition. Science. 2000;290:134–138.
15. Selleri C, Maciejewski JP, Sato T, Young NS. Interferon-gamma constitutively expressed in the stromal microenvironment of human marrow cultures mediates potent hematopoietic inhibition. Blood. 1996;87:4149–4157.
16. Okitsu Y, Takahashi S, Minegishi N, et al. Regulation of adipocyte differentiation of bone marrow stromal cells by transcription factor GATA-2. Biochem Biophys Res Commun. 2007;364:383–387.
17. Tremain N, Korkko J, Ibberson D, Kopen GC, DiGirolamo C, Phinney DG. MicroSAGE analysis of 2,353 expressed genes in a single cell-derived colony of undifferentiated human mesenchymal stem cells reveals mRNAs of multiple cell lineages. Stem Cells. 2001;19:408–418.

VOLUME 27 · NUMBER 36 · DECEMBER 20 2009

JOURNAL OF CLINICAL ONCOLOGY

ORIGINAL REPORT

Mutations of E3 Ubiquitin Ligase *Cbl* Family Members Constitute a Novel Common Pathogenic Lesion in Myeloid Malignancies

Hideki Makishima, Heather Cazzolli, Hadrian Szpurka, Andrew Dunbar, Ramon Tiu, Jungwon Huh, Hideki Muramatsu, Christine O'Keefe, Eric Hsi, Ronald L. Paquette, Seiji Kojima, Alan F. List, Mikkael A. Sekeres, Michael A. McDevitt, and Jaroslaw P. Maciejewski

From the Departmenst of Translational Hematology and Oncology Research and Hematologic Oncology and Blood Disorders, Taussig Cancer Institute; Department of Clinical Pathology, Cleveland Clinic, Cleveland, OH; Department of Laboratory Medicine, Ewha Woman's University, School of Medicine, Seoul, South Korea; University of California Los Angeles, Los Angeles, CA; H. Lee Moffitt Cancer Center, Tampa, FL; Division of Hematology and Hematological Malignancy, Department of Medicine and Oncology, Johns Hopkins University School of Medicine, Baltimore, MD; and the Department of Pediatrics, Nagoya University Graduate School of Medicine, Nagoya, Japan.

Submitted April 23, 2009; accepted August 6, 2009; published online ahead of print at www.jco.org on November 9, 2009.

Supported by in part by Grants No. RO1HL-082983, U54 RR019391 (J.P.M., M.A.S.), K24 HL-077522, DOD-MP048018 (M.A.M.), and by a grant from Aplastic Anemia & MDS International Foundation and Robert Duggan Charitable Fund (J.P.M.).

Authors' disclosures of potential conflicts of interest and author contributions are found at the end of this article.

Corresponding author: Jaroslaw P. Maciejewski, MD, PhD, Taussig Cancer Institute/R40, 9500 Euclid Ave, Cleveland OH 44195; e-mail: maciejj@ccf.org.

The Appendix is included in the full-text version of this article, available online at www.jco.org. It is not included in the PDF version (via Adobe® Reader®).

0732-183X/09/2736-6109/$20.00

DOI: 10.1200/JCO.2009.23.7503

ABSTRACT

Purpose
Acquired somatic uniparental disomy (UPD) is commonly observed in myelodysplastic syndromes (MDS), myelodysplastic/myeloproliferative neoplasms (MDS/MPN), or secondary acute myelogenous leukemia (sAML) and may point toward genes harboring mutations. Recurrent UPD11q led to identification of homozygous mutations in *c-Cbl*, an E3 ubiquitin ligase involved in attenuation of proliferative signals transduced by activated receptor tyrosine kinases. We examined the role and frequency of *Cbl* gene family mutations in MPN and related conditions.

Methods
We applied high-density SNP-A karyotyping to identify loss of heterozygosity of 11q in 442 patients with MDS, MDS/MPN, MPN, sAML evolved from these conditions, and primary AML. We sequenced *c-Cbl*, *Cbl-b*, and *Cbl-c* in patients with or without corresponding UPD or deletions and correlated mutational status with clinical features and outcomes.

Results
We identified *c-Cbl* mutations in 5% and 9% of patients with chronic myelomonocytic leukemia (CMML) and sAML, and also in CML blast crisis and juvenile myelomonocytic leukemia (JMML). Most mutations were homozygous and affected *c-Cbl*; mutations in *Cbl-b* were also found in patients with similar clinical features. Patients with *Cbl* family mutations showed poor prognosis, with a median survival of 5 months. Pathomorphologic features included monocytosis, monocytoid blasts, aberrant expression of phosphoSTAT5, and c-kit overexpression. Serial studies showed acquisition of *c-Cbl* mutations during malignant evolution.

Conclusion
Mutations in the *Cbl* family RING finger domain or linker sequence constitute important pathogenic lesions associated with not only preleukemic CMML, JMML, and other MPN, but also progression to AML, suggesting that impairment of degradation of activated tyrosine kinases constitutes an important cancer mechanism.

J Clin Oncol 27:6109-6116. © 2009 by American Society of Clinical Oncology

INTRODUCTION

Mutations and genomic aberrations constitute key pathogenic lesions in myeloid malignancies. In primary acute myelogenous leukemia (pAML) and chronic myelogenous leukemia (CML), reciprocal translocations have enhanced our understanding of molecular pathogenesis, improved diagnosis and provided rational therapeutic targets. In myelodysplastic syndromes (MDS), myelodysplastic/myeloproliferative neoplasms (MDS/MPN), and AML evolved from MDS or MDS/MPN (secondary AML [sAML]), unbalanced chromosomal lesions predominate and loss of heterozygosity (LOH) is of particular importance. LOH can arise either via hemizygous deletion, where a DNA segment is lost from one homolog while the other remains at one copy per cell, or by uniparental disomy (UPD), wherein the retained homolog is duplicated to preserve two total copies per cell at the locus. Thus, analysis of recurrent regions of LOH may point toward the presence of important mutations. Mutations seen in MDS and AML affect specific classes of genes and indicate general pathways of leukemia evolution.[1] For example, mutations have been found in a variety of receptor tyrosine kinases, including *c-Kit*, *c-Mpl*, and *Flt-3*.[2-4] Mutations also affect signal transduction genes such as *Jak2* and

NPM-1. *tP53* constitutes an example of a proapoptotic tumor suppressor gene mutated in aggressive leukemias.[5-7]

Until recently, metaphase cytogenetics was applied for detection of chromosomal defects including deletions resulting in LOH. Using this technique, a number of invariant chromosomal abnormalities have been described and minimal affected regions delineated, pointing towards potentially pathogenic genes. Single nucleotide polymorphism array (SNP-A) –based cytogenetic analysis allows for better resolution of chromosomal defects, with identification of previously cryptic unbalanced lesions.[8] In particular, SNP-A is able to identify UPD. We and others have recently shown that somatic UPD affecting various chromosomes can be found frequently in MDS, MDS/MPN, and sAML and have identified a number of recurrent areas.[9-11] Initially, UPD9p was shown to lead to homozygosity of the *Jak2* V617F mutation in MPN.[12-14] Using SNP-A, we have demonstrated that other areas of UPD can also be associated with homozygous mutations, including UPD13p (*Flt-3* ITD) and UPD1p (*c-Mpl*).[15,16] Based on this paradigm, we recently identified a novel recurrent area of UPD at 11q, frequently present in chronic myelomonocytic leukemia (CMML) and AML evolved from atypical MDS/MPN, and through delineation of a commonly deleted region have identified mutations in *c-Cbl*.[15] *c-Cbl* is an E3 ubiquitin ligase involved in degradation of activated receptor tyrosine kinases and other tyrosine kinases, including Src kinases. Consequently, mutations affecting the RING finger domain (RFD) may have a wide range of effects on proliferation regulation, crucial to both MPN and AML. In animal studies, *c-Cbl* knockout led to hyper-responsiveness to ligand stimulation and expansion of them in cell pools, overall resulting in a mild proliferative phenotype.[17] However, RFD mutation knock-in in a *c-Cbl*−/− mouse model resulted in a myeloproliferative phenotype and leukemic evolution (W.Y. Langdon, personal communication, December 2008). In a transgenic MDS NUP98/HOX13 mouse model, progression to sAML with acquisition of *RAS* and *c-Cbl* mutations occurs frequently.[18]

We hypothesized that mutations inactivating oncogene degradation pathways may constitute a new class of molecular lesions in myeloid malignancies modifying current paradigms of leukemogenesis. We therefore investigated the presence of mutations in the *Cbl* family of E3 ubiquitin ligases in selected subtypes of malignant myeloid disorders and determined the phenotypic and functional features as well as clinical outcomes. Based on the study of these features we set out to discern the pathophysiologic principles of molecular dysfunction created by E3 ubiquitin ligase lesions.

METHODS

Patients

Bone marrow aspirates were collected from 442 patients with MDS (n = 115), MDS/MPN (n = 98), MPN (n = 22), sAML (n = 110) evolved from these conditions, and pAML (n = 97) seen at Cleveland Clinic and Johns Hopkins Hospital between 2003 and 2008 (Appendix Table A1, online only). Informed consent for sample collection was obtained according to protocols approved by institutional review boards. Diagnosis was confirmed at each primary institution and assigned according to WHO classification criteria.[19]

Single Nuclotide Polymorphism Array Analysis

High-density Affymetrix SNP-A (250K and 6.0 arrays; Affymetrix, Santa Clara, CA) were applied as a karyotyping platform to identify LOH on chromosome 11q. Lesions identified by SNP-A were compared to the Database of Genomic Variants[20] (http://projects.tcag.ca/variation/) and an internal control series (n = 1,003) to exclude known copy number variations. To confirm all regions of LOH detected by 250K SNP-A, we repeated samples when possible on 6.0 arrays and analyzed using Genotyping Console version 2.0 (Affymetrix). Signal intensity was analyzed and SNP calls determined using Gene Chip Genotyping Analysis Software version 4.0 (GTYPE, Affymetrix). Copy number and areas of UPD were investigated using a Hidden Markov Model and CN Analyzer for Affymetrix GeneChip Mapping 250K arrays (CNAG version 3.0) as previously described.[21]

E_3 Ubiquitin Ligase Mutational Screening

To screen patients for mutations in *c-Cbl*, *Cbl-b*, *Cbl-c*, and *Hakai*, direct genomic sequencing of all exons was performed (details of primers and conditions are available on request). For sequencing, 250 ng of polymerase chain reaction (PCR) product, 3 μmol/L original forward or reverse primer, 2 μL Big Dye version 3.1 (Applied Biosystems, Foster City, CA), and 14.5 μL deionized H_2O were amplified under the following conditions: 95°C (2 minutes) followed by 25 cycles of 95°C (10 seconds), 50°C (5 seconds), and 60°C (4 minutes). Sequencing was performed as previously described.[15] If a mutation was intronic, RNA was extracted by TRIzol (Invitrogen, Carlsbad, CA) and reverse transcription polymerase chain reaction performed for confirmation of splice variants.

Immunohistochemical Detection of $pSTAT_5$

Staining was performed on a Benchmark XT platform (Ventana Medical Systems, Tucson, AZ), according to the manufacturer's instructions, using mouse monoclonal antiphospho-STAT5a/b (Y694/99; Advantex BioReagents LLP, Conroe, TX) at 1:500 dilution. All stains were scored without knowledge of the clinical diagnosis or mutational status. Phospho-STAT5-positive staining (nMEG pSTAT5) was defined as previously reported.[22,23] Images were obtained via digital microscopy using an Olympus BX51 microscope (Olympus America, Melville, NY) equipped with either a UPlanFl 40×/0.75 numeric aperture (NA) or a UPlanFl 100 ×/1.30 NA objective. Images were captured using a Dage-MTI Model DC330E charge-coupled device camera (Dage-MTI, Michigan City, IN) attached to the microscope with a U-TV1X-2 video adapter (Olympus America) and a 0.45× camera coupler (Diagnostic Instruments, Sterling Heights, MI).

Statistical Analysis

Overall survival was defined as the time a patient was diagnosed with a myeloid malignancy at Cleveland Clinic or Johns Hopkins to death or last known contact, and analyzed using Kaplan-Meier statistics and Cox's proportional hazards model. For comparison of the frequency of clinical features between *Cbl* family mutation and wild-type (WT), categoric variables were analyzed using Fisher's exact test.

RESULTS

Detection of UPD11q Using SNP-A and Detection of c-Cbl Mutation

Previously, we identified homozygous *c-Cbl* mutations in patients with CMML and UPD11q.[15] Using SNP-A karyotyping, we studied a large cohort of patients (n = 442) with MDS and related disorders, including JMML and CML blast crisis (CML-BC), to assess the frequency of this lesion within clinical subtypes. Three hundred one and 187 cases were examined by 250K and 6.0 arrays, respectively. Forty-six cases were analyzed using both arrays, yielding identical results. Based on the analysis of 1,003 controls, we determined the average size and location of nonclonal regions of autozygosity. All of these nonclonal regions were interstitial. For the purpose of this study, we have excluded all regions of autozygosity based on the size criteria (27 Mb) derived from controls. The remaining regions were confirmed by analysis of germ-line samples (nonclonal CD3+ lymphocytes) in 45 patients (Fig 1A). Regions of homozygosity found in both

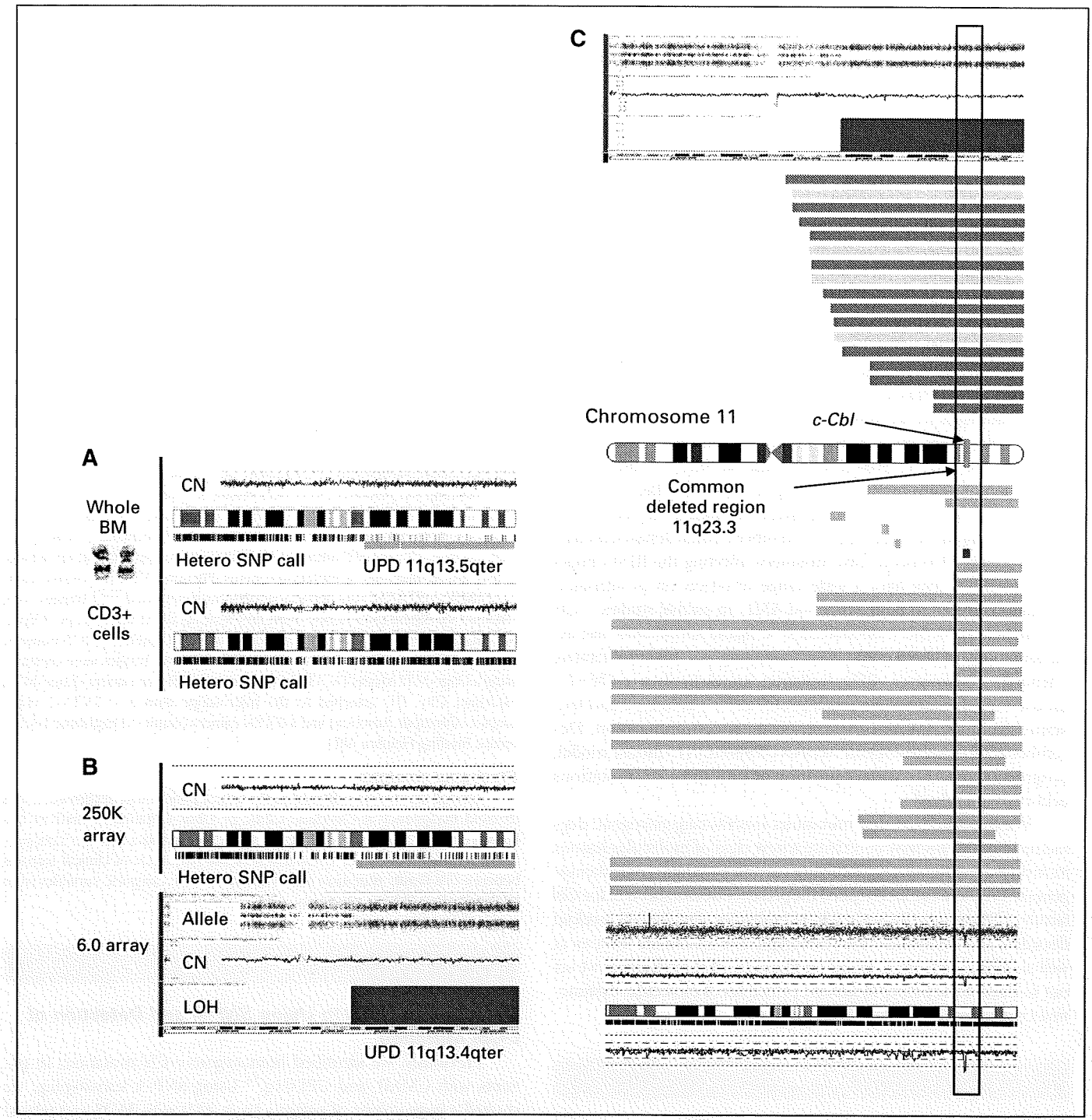

Fig 1. Detecting acquired, segmental uniparental disomy (UPD) using single nucleotide polymorphism array (SNP-A) technology. (A) SNP-A karyograms of both whole bone marrow (BM) cells and CD3+ lymphocytes of a patient show the somatic nature of acquired UPD in chromosome 11. The blue line represents average copy number (CN) signal intensity of SNPs on the array chip. In this instance, there are no CN variations, and thus, the blue line does not deviate from normal diploid CN. The green marks below the idiogram represent heterozygosity at particular DNA loci. In the region of UPD seen in whole BM cells, drastic reduction of heterozygous loci denotes the region of UPD (pink bar). The remaining green marks in the region of UPD delineate the presence of nonclonal cells in the sample. An abnormal chromosome 11 was not detected when metaphase cytogenetic analysis was performed on bone marrow. In CD3+ sorted lymphocytes, a normal chromosome 11 is seen. (B) Comparison of Affymetrix 250K and 6.0 arrays in the detection of UPD11q. CNAG version 3.0 analysis (top) shows clear UPD of chromosome 11 by loss of heterozygous loci. Repeated testing on the 6.0 array and analysis using Genotyping Console v2.0 software (bottom) confirms the 250K SNP-A findings. Note that the Genotyping Console output includes allele difference, loss of heterozygosity (LOH), and CN variation plots. The allele difference graph represents the genotypes for each individual SNP. Dots with a value of 1 represent SNPs with an AA genotype, whereas those with a value of −1 represent SNPs with a BB genotype. Dots at 0 represent heterozygous SNPs (AB). Complete loss of all AB SNPs indicates copy-neutral LOH. This is further shown by both the LOH and CN graphs, which show no loss in CN but clear LOH. (C) Topographic maps show regions of (red) UPD or (green) deletion in individual patients on chromosome 11q. Bars corresponding to the ideogram represent the regions affected for each patient. The *c-Cbl* locus was included in the common deleted region (11q23.3) among UPDs and deletions. Red and pink bars represent UPD lesions with and without *c-Cbl* mutations, while dark and light green bars show deletions with and without mutations. Top is 6.0 array karyogram with UPD11q and bottom is one with microdeletion 11q by 250K array analysis. *c-Cbl* mutations were identified in both cases.

bone marrow and CD3+ fractions were excluded from further analyses. We confirmed UPD11q detected on 250K arrays by repeated analyses using ultra-high density Affymetrix 6.0 arrays and Genotyping Console version 2.0 software (Fig 1B). Among a total of 133 regions of somatic UPD on multiple chromosomes including 1, 4, 17, and 21, UPD11q was most common (n = 17). LOH can also result from deletions, and deletions involving 11q23.3 were found in 29 patients (Fig 1C). Sequencing *c-Cbl* revealed mutations in 13 cases (76%) of UPD11q. However, among patients with deletion11q, a *c-Cbl* mutation was found in only one case (CMML). We also analyzed patients without LOH11q to assess the frequency of heterozygous mutations and identified five cases (1.2%).

c-Cbl *Mutations and Clinical Features*

We sequenced all exons of *c-Cbl*; all mutations, except for 1 frame shift mutation in the tyrosine kinase–binding domain, were associated with the RFD or linker sequence, which are highly conserved among species. More importantly, 12 mutations in the RFD were located at or next to a cysteine residue (63%; Fig 2). The presence of each somatic mutation was confirmed by bidirectional DNA sequencing of multiple isolates and comparison against CD3+ sorted lymphocytes when possible.

In one case of a patient with MDS (refractory anemia subtype) and monosomy 7 who transformed to AML, SNP-A karyotyping revealed the UPD11q, yet after transformation to AML sequencing identified a *c-Cbl* mutation creating a novel splice site resulting in a longer transcript (Appendix Fig A1, online only). We also found a hemizygous mutation in the linker sequence in a CMML patient with a microdeletion of 11q23.3 previously undetected by metaphase cytogenetics (Appendix Fig A2, online only). Eleven mutations were found in CMML and similar forms of MDS/MPN unclassifiable either at or before the time of testing; 6 of these patients progressed to sAML (55%). In total, two (5%) of 38 patients with CMML, 10 (9%) of 110 with sAML, and one (1%) of 115 patients with MDS carried mutant *c-Cbl* (Appendix Table A2, online only). In addition, *c-Cbl* mutations were found in four (19%) of 21 patients with JMML and one (10%) of 10 with CML-BC.

Other Mutations and Nonsynonimous SNPs in Related E_3 Ubiquitin Ligases

The *Cbl* family contains several other E3 ligases, including *Cbl-b* (3q) and *Cbl-c* (19q) as well as a novel member with high homology called *Hakai* (7q). Based on structural and functional similarities we hypothesized that these genes can also harbor mutations associated with similar clinical phenotypes. When we sequenced 12 patients with corresponding UPDs, no mutations were found. However, when we sequenced all patients in our cohort without *c-Cbl* mutations, we identified three with a heterozygous and one with a hemizygous *Cbl-b* mutation (Appendix Fig A3, online only) and three patients (one cell line) with a *Cbl-c* frame shift polymorphism with a single base insertion, all affecting the RFD (Fig 2). In addition, we identified 12 (7%) of 167 patients with myeloid malignancies harboring another rare nonsynonymous SNP in *Cbl-c*, also affecting the RFD (H405Y). The frequency of this SNP in the general population is less than 1% (data not shown).

Clinical Characteristics in Patients With Cbl Family Mutation

In order to identify the pathologic subtypes in which *Cbl* family member mutations may play a role, we systematically investigated a wide range of myeloid malignancies. They were most commonly associated with MDS/MPN subentities, including CMML and atypical MDS/MPN, and some cases of typical MDS. In addition, *Cbl* family mutations appear to be present in sAML with an antecedent history of MDS/MPN. Based on this distribution of *c-Cbl* mutations, we analyzed other related disease entities within MDS/MPN and MPN; we also identified *c-Cbl* mutations in JMML and in CML-BC (Appendix Table A2). This pattern suggests that *c-Cbl* mutations can be a characteristic feature of atypical MDS/MPN syndromes or serve as a second genetic hit facilitating malignant

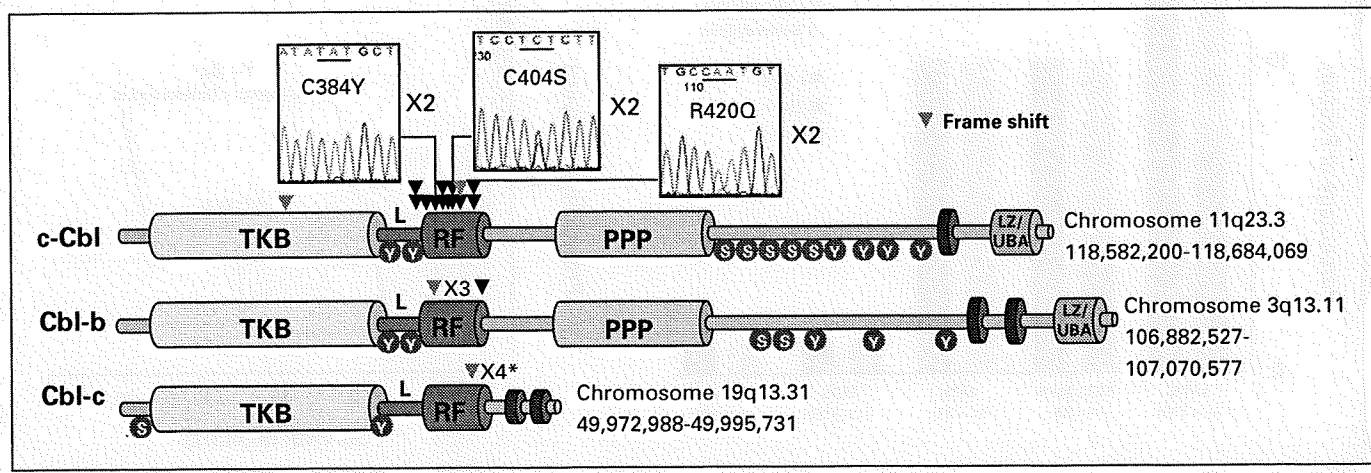

Fig 2. Identification of variations in *c-Cbl*, *Cbl-b* and *Cbl-c* RING finger (RF) domain. Schematic representation shows the major domains of *c-Cbl*, *Cbl-b*, and *Cbl-c*, primarily the tyrosine kinase binding (TKB) domain, linker sequence (L), RF domain, proline-rich region (PPP), and leucine zipper (LZ)/ubiquitin-associated domain (UBA). Tyrosine and serine residues, represented by red circles, are phosphorylated by tyrosine kinases. Genomic DNA sequencing of all exons in *c-Cbl*, *Cbl-b*, and *Cbl-c* revealed the presence of (black arrow) missense and (blue arrow) frame shift mutations or frame shift polymorphisms in L or RF domain, except for a case with a mutation in the TKB domain. In *c-Cbl*, some basepair changes occured in a homozygous state because of UPD and resulted in the substitution of cysteine or arginine residues at positions 384 shared in two patients (C384Y), 404 in three patients (C404S/Y), and 420 in three patients (R420Q/P). (*) Frame shift polymorphism.

